ARTICLE

Corrected: Author Correction

https://doi.org/10.1038/s41586-019-1485-8

Mechanosensation of cyclical force by PIEZO1 is essential for innate immunity

Angel G. Solis[1], Piotr Bielecki[1], Holly R. Steach[1], Lokesh Sharma[2], Christian C. D. Harman[3], Sanguk Yun[4,5,6], Marcel R. de Zoete[7], James N. Warnock[8], S. D. Filip To[9], Autumn G. York[1], Matthias Mack[10], Martin A. Schwartz[4,5,6], Charles. S. Dela Cruz[2], Noah W. Palm[1], Ruaidhrí Jackson[1]* & Richard A. Flavell[1,11]*

Direct recognition of invading pathogens by innate immune cells is a critical driver of the inflammatory response. However, cells of the innate immune system can also sense their local microenvironment and respond to physiological fluctuations in temperature, pH, oxygen and nutrient availability, which are altered during inflammation. Although cells of the immune system experience force and pressure throughout their life cycle, little is known about how these mechanical processes regulate the immune response. Here we show that cyclical hydrostatic pressure, similar to that experienced by immune cells in the lung, initiates an inflammatory response via the mechanically activated ion channel PIEZO1. Mice lacking PIEZO1 in innate immune cells showed ablated pulmonary inflammation in the context of bacterial infection or fibrotic autoinflammation. Our results reveal an environmental sensory axis that stimulates innate immune cells to mount an inflammatory response, and demonstrate a physiological role for PIEZO1 and mechanosensation in immunity.

Homeostatic host physiology shows substantial changes over the course of an immune response. In the context of inflammation, the microenvironment experiences robust alterations in temperature[1], oxygen availability[2], pH[40], osmolarity[3] and nutrient availability[4], which can direct distinct immunological responses. Immune cells can therefore tailor their response—not only to the pathogen they are exposed to or the pattern recognition receptors (PRRs) that are activated, but also using a number of microenvironmental sensors simultaneously—to enable a precise immune response that is optimized to a specific microenvironmental challenge. Although there has been progress in research on myeloid responses to PRR signalling and the sensing of fluctuations in the aforementioned environments[5], relatively little is known about the contribution of force and pressure to innate immunity[6]. Immune cells recruited to highly mechanical organs, such as the lung, are exposed to both tonic and dynamically changing mechanical cues. For example, innate immune cells experience shear stresses in the circulation during extravasation[7], membrane deformation during the transmigration process[6] and cyclical hydrostatic pressure (CHP) once they are fully infiltrated into the lung[8]. Therefore, although force and pressure are major physiological parameters capable of signalling to cells during these immunologically relevant processes, their contribution to immunity is almost completely unknown.

Here we identify the PIEZO1 ion channel[9] as a sensor of cyclical pressure in myeloid cells, which initiates a proinflammatory response. Mechanical stimulation of macrophages and monocytes triggers a potent and selective expression program of proinflammatory and chemoattractant mediators in vitro. This inflammatory mechanosensation response is entirely dependent on PIEZO1. Mechanistically, we show that recognition of CHP by PIEZO1 drives a Ca^{2+}-dependent activation of activating protein-1 (AP-1) and transcription of endothelin-1 (*Edn1*). EDN1 signalling in turn triggers stabilization of hypoxia-inducible factor 1α (HIF1α), facilitating the prolonged proinflammatory expression profile driven by CHP in myeloid cells. Mice that are conditionally deficient in Piezo1 in myeloid cells exhibit marked susceptibility to intranasal bacterial infection with *Pseudomonas aeruginosa*, characterized by impaired monocyte-dependent EDN1 expression, HIF1α-stabilization and production of proinflammatory mediators. Conversely, PIEZO1 signalling in myeloid cells exacerbates a model of pulmonary fibrosis, indicating that mechanosensation in the altered microenvironment of fibrotic tissue can itself potentiate autoinflammation and disease pathology. In sum, our results implicate force and pressure as major signals dictating innate immune driven inflammation.

Cyclical pressure sensing by PIEZO1 in myeloid cells

Mechanosensation in mammals affects and regulates a wide variety of processes including pain sensation in neuronal cells[10], epithelial cell division[11] and endothelial cell-mediated vasodilation[12]. These mechanical cues signal through a class of proteins known as mechanosensory ion channels (MSICs)[13]. To investigate myeloid-cell mechanosensation, we first investigated whether macrophages express any MSICs. Bone-marrow derived macrophages (BMDMs) showed high expression of PIEZO1, an ion channel with high affinity for calcium, and negligible levels of other reported MSICs (Fig. 1a). To identify the biological response to physical force in macrophages, cells were placed in a bioreactor capable of subjecting cells to CHP[14]. This pressure chamber consists of solenoid intake and exhaust valves to control the frequency of mechanostimulation, is connected to a gas tank filled with 5% CO_2 in air and is housed in a tissue culture incubator to equilibrate to physiological temperature (Extended Data Fig. 1a). BMDMs were subjected to CHP at an amplitude of 15 mm Hg, cycling

[1]Department of Immunobiology, Yale University School of Medicine, New Haven, CT, USA. [2]Department of Internal Medicine, Pulmonary, Critical Care and Sleep Medicine, Yale School of Medicine, New Haven, CT, USA. [3]Department of Genetics, Yale University School of Medicine, New Haven, CT, USA. [4]Department of Internal Medicine (Cardiology), Yale Cardiovascular Research Center, Yale University, New Haven, CT, USA. [5]Department of Cell Biology, Yale Cardiovascular Research Center, Yale University, New Haven, CT, USA. [6]Department of Biomedical Engineering, Yale Cardiovascular Research Center, Yale University, Yale University, New Haven, CT, USA. [7]Department of Infectious Diseases and Immunology, Utrecht University, Utrecht, The Netherlands. [8]School of Chemical, Materials and Biomedical Engineering, University of Georgia, Athens, GA, USA. [9]Department of Agricultural and Biological Engineering, Mississippi State University, Mississippi State, MS, USA. [10]Department of Internal Medicine II—Nephrology, University Hospital Regensburg, Regensburg, Germany. [11]Howard Hughes Medical Institute, Yale University, New Haven, CT, USA. *e-mail: ruaidhri.jackson@yale.edu; richard.flavell@yale.edu

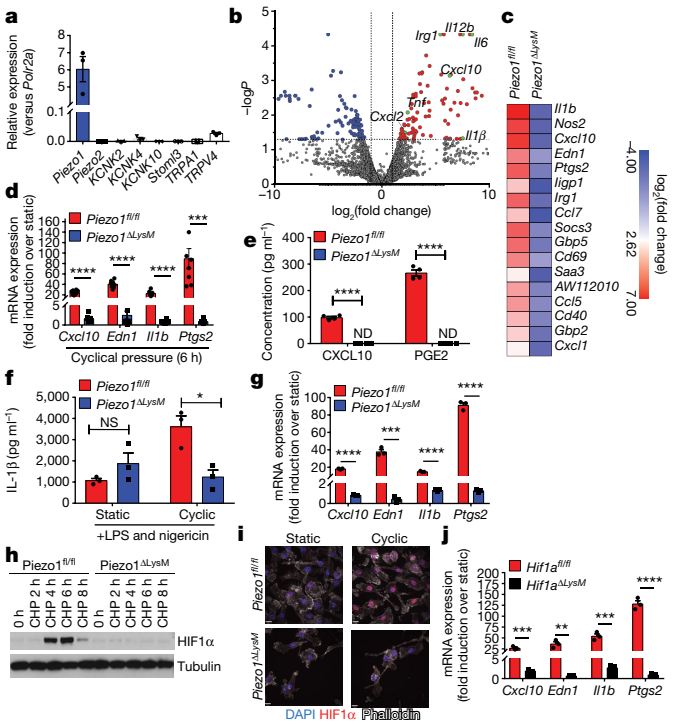

Fig. 1 | PIEZO1 signalling in macrophages induces transcriptional reprogramming via HIF1α. a, RT–qPCR analysis of known mammalian mechanosensory ion channels from unstimulated BMDMs. Data are presented as three biological replicates from two independent experiments. **b**, Volcano plots showing differentially expressed genes in *Piezo1*$^{fl/fl}$ BMDMs cultures with 6 h of CHP over static pressure. **c**, Heat map showing top genes upregulated by PIEZO1 signalling. Data are shown as $\log_2$ fold change of CHP-treated over static pressure-treated *Piezo1*$^{fl/fl}$ or *Piezo1*$^{\Delta LysM}$ BMDMs 6 h after mechanostimulation. **d**, RT–qPCR analysis of top upregulated genes from BMDMs treated with 6 h of cyclic hydrostatic pressure. Data are presented as eight biological replicates from three independent experiments. **e**, ELISA of CXCL10 and PGE2 from supernatant of BMDMs cultured with CHP or static pressure for 6 h. Data are presented as four biological replicates from two independent experiments. **f**, IL-1β levels from BMDMs treated with 5 h of LPS (10 ng ml^{-1}) and 1 h of nigericin (10 μM) with CHP or static pressure, as measured by ELISA. Data are presented as three biological replicates. **g**, RT–qPCR validation of top upregulated genes from purified mouse monocytes treated with 6 h CHP. Data are presented as three biological replicates. **h**, Immunoblot analysis of HIF1α and β-tubulin in BMDMs cultured with CHP for the indicated time. Blots are representative of five independent experiments. **i**, Immunofluorescence of HIF1α from BMDMs cultured with CHP or static pressure for 6 h. Data are representative of two independent experiments. **j**, RT–qPCR analysis of *Hif1a*$^{fl/fl}$ and *Hif1a*$^{\Delta LysM}$ BMDMs treated with 6 h CHP. Data are presented as three biological replicates. Data in **a**, **d**–**g**, **j** are mean ± s.e.m.; unpaired two-tailed *t*-test (**$P < 0.01$, ***$P < 0.001$ and ****$P < 0.0001$). NS, not significant.

once per second (Extended Data Fig. 1b). As a control, cells were placed in the chamber with a noncyclic pressure (that is, static pressure) (Extended Data Fig. 1b). Because PIEZO1 deficiency is embryonically lethal[15], we crossed *Piezo1*-floxed mice to LysM-Cre mice to delete PIEZO1 in myeloid cells. BMDMs from *Piezo1*$^{\Delta LysM}$ showed approximately 95% reduction in *Piezo1* mRNA compared with *Piezo1*$^{fl/fl}$ cells (Extended Data Fig. 1c). To observe any biological response to mechanostimulation, BMDMs from *Piezo1*$^{fl/fl}$ and *Piezo1*$^{\Delta LysM}$ mice were incubated in the pressure chamber for 6 h and subjected to RNA-sequencing analysis (RNA-seq). CHP triggered robust upregulation of proinflammatory genes such as *Il1b*, *Cxcl10* and *Ptgs2* in *Piezo1*$^{fl/fl}$ macrophages (Fig. 1b). However, this transcriptional reprogramming was completely abrogated in *Piezo1*$^{\Delta LysM}$ BMDMs (Fig. 1c). We then validated the most upregulated genes by reverse transcription with quantitative PCR (RT–qPCR) and enzyme-linked immunosorbency assay (ELISA) (Fig. 1d–f). Furthermore, as increasing the overall magnitude of static pressure failed to induce transcriptional reprograming, we conclude that macrophage PIEZO1 responds to CHP rather than the overall magnitude of the force (Extended Data Fig. 1d, e). Additionally, cultured monocytes showed similar transcriptional reprogramming following CHP treatment, indicating a conserved PIEZO1-mediated mechanosensation-signalling axis in myeloid cells. (Fig. 1g). As *Il1b* was upregulated following PIEZO1 signalling, we investigated whether CHP influences inflammasome activation. Canonically, the NLRP3 inflammasome is first primed, usually via lipopolysaccharide (LPS), to transcriptionally upregulate *Il1b* and *Nlrp3*[16]. The primed inflammasome is then activated via a second signal that leads to Ca^{2+} influx and K^+ efflux[16]. It is possible that PIEZO1 signalling can substitute for either signal; however, CHP alone was not sufficient to induce IL-1β release in the absence of either LPS or nigericin (Extended Data Fig. 1f). This is probably because CHP does not induce upregulation of *Nlrp3* (Fig. 1b, c). Together these results indicate that myeloid cells can not only sense CHP alterations in their environment via PIEZO1, but can also also functionally integrate this signal to drive a potent and selective proinflammatory response even in the absence of classical pathogen-associated molecular patterns.

To investigate the mechanistic signalling program(s) that underly this proinflammatory activation, we examined potential transcription factors that could explain the gene upregulation. We observed that a number of the upregulated genes were targets of HIF proteins[17–19]. Indeed, BMDMs from *Piezo1*$^{fl/fl}$ mice displayed accumulation of HIF1α protein 4–6 h after CHP stimulation; BMDMs from *Piezo1*$^{\Delta LysM}$ mice displayed no such accumulation (Fig. 1h). Furthermore, upon mechanostimulation, HIF1α translocated to the nucleus only in *Piezo1*$^{fl/fl}$ BMDMs (Fig. 1i). To test the dependence of HIF1α on the observed transcriptional reprogramming, we crossed *Hif1a*$^{fl/fl}$ and LysM-Cre mice to generate BMDMs deficient in HIF1α. HIF1α-deficient macrophages showed complete abrogation of CHP-induced transcriptional reprograming (Fig. 1j). In normoxic conditions, HIF1α hydroxylation by prolyl hydroxylases (PHDs) marks HIF1α for ubiquitination via the Von Hippel Lindau tumour suppressor E3 ubiquitin ligase and, ultimately, for degradation[20]. To investigate whether the pressure chamber generated a hypoxic environment, we used pimonidazole, which forms a detectable product only in the absence of oxygen[21]. BMDMs cultured for 6 h in hypoxic conditions (2% O_2) showed a clear increase in detectable pimonidazole, but no HIF1α stabilization was seen at this early time point (Extended Data Fig. 2a). By contrast, no detectable pimonidazole was detected following static or CHP conditions (Extended Data Fig. 2b). In addition, hypoxic conditions did not recapitulate the observed transcriptional upregulation of proinflammatory genes, nor did it synergize with PIEZO1 signalling (Extended Data Fig. 2c). Furthermore, we did not detect a difference in *Hif1a* mRNA levels following CHP (Extended Data Fig. 2d). Therefore, we conclude that PIEZO1 signalling results in stabilization of HIF1α.

PIEZO1 stabilizes HIF1α via EDN1 in myeloid cells

We next sought to determine how PIEZO1 signalling results in HIF1α stabilization. We first investigated whether CHP inhibits PHD enzymes globally. In contrast to HIF1α, CHP did not trigger HIF2α stabilization (Extended Data Fig. 2e), demonstrating that recognition of CHP by myeloid cells specifically regulates HIF1α degradation. Acidic pH also induces HIF1α stabilization[22]; however, CHP had no effect on intracellular or extracellular acidity (Extended Data Fig. 3). PIEZO1 functions as an ion channel, facilitating calcium influx into the cytoplasm[23,24]. To test whether PIEZO1-dependent calcium influx was the driver of HIF1α in BMDMs, cells were subjected to CHP in calcium-free medium or with the addition of the PIEZO1 inhibitor GsMTx4. The HIF1α signal was completely abrogated in both conditions, suggesting that PIEZO1 mediates HIF1α accumulation via Ca^{2+} influx in response to CHP (Fig. 2a). Furthermore, the reversible GsMTx4 PIEZO1 inhibitor could be washed off the cells, restorating HIF1α stabilization,

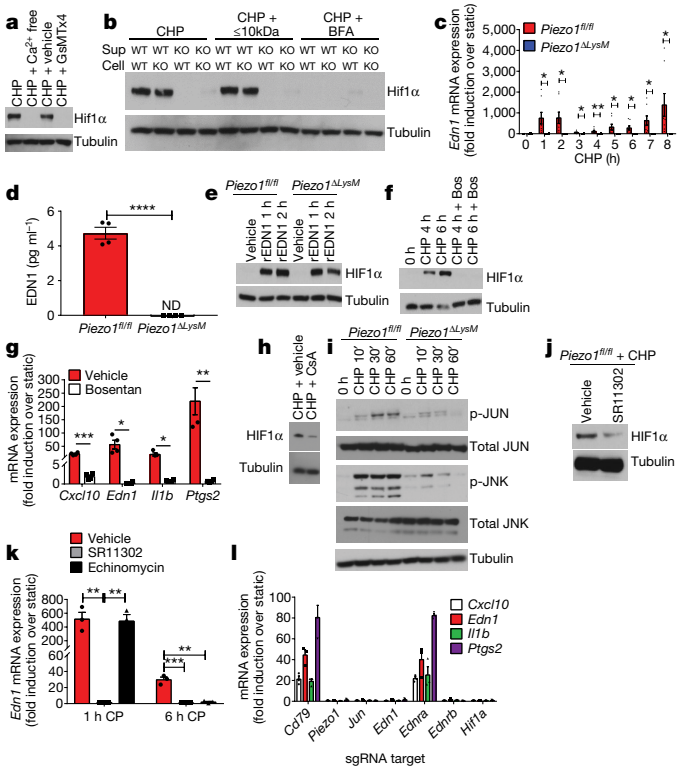

Fig. 2 | PIEZO1 signalling stabilizes HIF1α via EDN1. a, Immunoblot analysis of HIF1α and β-tubulin in BMDMs cultured under CHP for 6 h with calcium-free medium or with the PIEZO1 inhibitor GsMTx4 (5 μM). Blots are representative of two independent experiments. **b**, Immunoblot analysis of HIF1α and β-tubulin in BMDMs. Supernatant (sup) from *Piezo1*$^{fl/fl}$ (WT) or *Piezo1*$^{\Delta LysM}$ (KO) BMDMs cultured with 6 h CHP were transferred to *Piezo1*$^{fl/fl}$ or *Piezo1*$^{\Delta LysM}$ BMDMs and cultured under static pressure for 2 h. Molecules larger than 10 kDa were removed using a size-exclusion spin column. Secretion was inhibited using brefeldin A (3 μg ml^{-1}). Blots are representative of two independent experiments. **c**, RT–qPCR analysis of *Edn1* from CHP-treated BMDMs. Data are presented as eight biological replicates from three independent experiments. **d**, ELISA of EDN1 in supernatants from BMDMs cultured with 6 h CHP. Data are presented as four biological replicates from two independent experiments. **e**, Immunoblot analysis of HIF1α and β-tubulin in BMDMs treated with 10 nM rEND1. Blots are representative of three independent experiments. **f**, Immunoblot analysis of HIF1α and β-tubulin in BMDMs with CHP for 6 h in the presence of 10 μM bosentan (bos). Blots are representative of three independent experiments. **g**, RT–qPCR analysis of *Piezo1*$^{fl/fl}$ BMDMs pretreated with 10 μM bosentan for 30 min before 6 h CHP. Data are presented as four biological replicates. **h**, Immunoblot analysis of HIF1α and β-tubulin in BMDMs pretreated with 10 μM cyclosporin A for 30 min before 6 h CHP. Blots are representative of two independent experiments. **i**, Immunoblot analysis of phospho- JUN (p- JUN), phospho-JNK (p-JNK), total JUN, total JNK and β-tubulin in BMDMs cultured under CHP for indicated time periods. Blots are representative of three independent experiments. **j**, Immunoblot analysis of HIF1α and β-tubulin in BMDMs pretreated with the AP-1 inhibitor SR11302 (10 μM) for 30 min before 6 h CHP. Blots were representative of two independent experiments. **k**, RT–qPCR analysis of *Edn1* from BMDMs pretreated with either 10 μM SR11302 or 5 nM echinomycin for 30 min before 6 h CHP. Data are presented as three biological replicates. **l**, RT–qPCR analysis of Cas9-KI BMDMs transduced with sgRNAs targeting the indicated gene of interest after 6 h CHP. Data are presented as three biological replicates. Data in **c**, **d**, **g**, **k**, **l** are mean ± s.e.m.; significance is determined by unpaired two-tailed *t*-test (*$P < 0.05$, **$P < 0.01$, ***$P < 0.001$ and ****$P < 0.0001$).

indicating an operative role for the PIEZO1 channel in Ca^{2+} influx (Extended Data Fig. 4a). Indeed, as depletion of intracellular calcium stores with the cell-permeable calcium chelator BAPTA-AM had no effect on HIF1α stabilization (Extended Data Fig. 4b), we conclude that Ca^{2+} derived from the extracellular space via PIEZO1 is required for CHP-dependent HIF1α stabilization.

To test whether HIF1α stabilization was caused by a secreted soluble factor, we performed supernatant-transfer experiments. In brief, *Piezo1*$^{fl/fl}$ and *Piezo1*$^{\Delta LysM}$ BMDMs were cultured for 6 h under CHP. Supernatant was then clarified and transferred to fresh cells under static pressure for 2 h. Supernatant from CHP-treated *Piezo1*$^{fl/fl}$ BMDMs could stabilize HIF1α in both *Piezo1*$^{fl/fl}$ and *Piezo1*$^{\Delta LysM}$ macrophages, whereas supernatant from *Piezo1*$^{\Delta LysM}$ was unable to do so (Fig. 2b). Additionally, using size-exclusion chromatography and brefeldin A, we showed that the stabilizing factor is smaller than 10 kDa and is secreted through the vesicular system (Fig. 2b). We were able to wash BFA from the medium and observe restoration of HIF1α 2 h later (Extended Data Fig. 4c). Together, these data support a model in which PIEZO1-dependent Ca^{2+} signalling drives expression of a small secretory molecule with the ability to stabilize HIF1α.

We therefore re-examined the RNA-seq data to identify possible gene targets of PIEZO1 signalling. EDN1 is a hormone that causes vasoconstriction in endothelial cells[25]. PIEZO1 signalling resulted in robust upregulation and secretion of EDN1 (Fig. 2c, d). Translation and processing of EDN1 in the Golgi results in a biologically active 2-kDa peptide[25]. Secretion of active EDN1 is therefore blocked by BFA and stabilizes HIF1α in smooth muscle cells in vitro[26]. *Edn1* upregulation occurred as quickly as 1 h after CHP stimulation (Fig. 2c) and recombinant EDN1 stabilized HIF1α in both *Piezo1*$^{fl/fl}$ and *Piezo1*$^{\Delta LysM}$ macrophages (Fig. 2e). The endothelin receptor antagonist bosentan completely blocked HIF1α stabilization with CHP and prevented the observed transcriptional reprogramming following mechanostimulation (Fig. 2f, g). Mechanistically, EDN1 stabilizes HIF1α by activating calcineurin, which dephosphorylates RACK1[26]. RACK1 phosphorylation is necessary to bring HIF1α in contact with E3-ubiquitin ligases responsible for subsequent proteasomal degradation[27]. To test whether this mechanism is relevant in CHP-stimulated macrophages, we used cyclosporin A, an inhibitor of calcineurin[26]. Treatment with CsA during CHP treatment resulted in a loss of HIF1α stabilization, suggesting that this mechanism is conserved in macrophages following CHP stimulation (Fig. 2h). In agreement with these results, HIF1α stabilization in *Piezo1*$^{\Delta LysM}$ BMDMs is rescued by the proteasome inhibitor MG132 but not with chloroquine, a lysosomal-acidification inhibitor (Extended Data Fig. 4d).

We next sought to understand the early PIEZO1-dependent signalling pathway that drives the primary EDN1 upregulation (Fig. 2c). Inhibition of HIF1α had no effect on *Edn1* at early time points (Extended Data Fig. 4e). Cyclical mechanotransduction has been reported to activate EDN1 expression via AP-1 through an unknown sensory mechanism[28]. At early time points of CHP, we observed PIEZO1-dependent phosphorylation of JNK and JUN (Fig. 2i). Pharmacological inhibition of AP-1 resulted in destabilization of HIF1α 6 h after mechanostimulation, and loss of *Edn1* at 1 h and 6 h of CHP treatment (Fig. 2j, k). Of note, however, treatment with echinomycin—an inhibitor of HIF1α–DNA interactions—resulted in loss of *Edn1* only at the 6 h time point (Fig. 2k), indicating that AP-1 is the early driver of EDN1 and HIF1α is a late driver that is sufficient to potentiate the proinflammatory transcriptional program. However, HIF1α stabilization alone via the PHD inhibitor DMOG is insufficient to drive the transcriptional response (Extended Data Fig. 4f, g). We reasoned that CHP may prime targets of HIF1α into a state that allows for robust transactivation. To test this, we stimulated BMDMs with CHP for 2 h before DMOG treatment and observed robust transcriptional reprogramming that was abrogated with static pressure or in the absence of DMOG (Extended Data Fig. 4f, g). Finally, using Cas9-knockin (Cas9-KI) BMDMs, we disrupted key genes in the hypothesized signalling pathway to genetically validate our proposed mechanism. Single-guide RNAs were cloned into a retroviral vector, and transduction of Cas9-KI macrophages resulted in inactivation of the targeted gene[29]. Guide RNAs targeting *Piezo1*, *Jun*, *Edn1*, endothelin receptor B (*Ednrb*) or *Hif1a* resulted in a complete abrogation

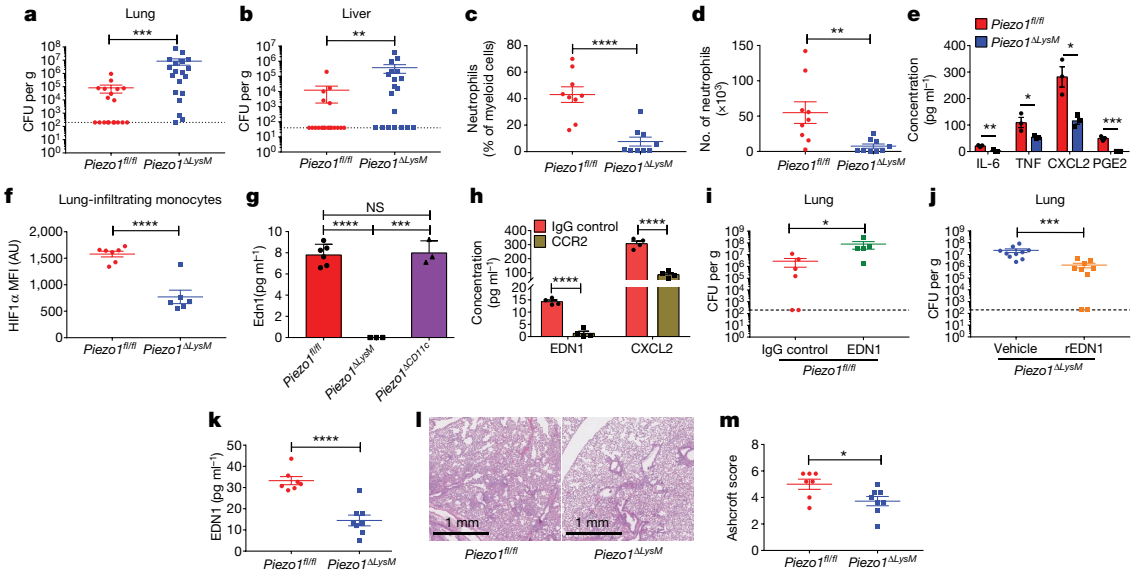

Fig. 3 | PIEZO1 recognition of the cyclical hydrostatic pressure microenvironment in the lung drives inflammation via EDN1. **a**, **b**, *P. aeruginosa* CFU counts from lung (**a**) and liver (**b**) of *Piezo1*$^{fl/fl}$ ($n = 19$) or *Piezo1*$^{\Delta LysM}$ ($n = 19$) mice, 24 h after intranasal infection with *P. aeruginosa*. Data are from four independent experiments. Dotted line, limit of detection. **c**, **d**, Neutrophil quantification as percentage of myeloid cells (**c**) and total numbers (**d**) from *Piezo1*$^{fl/fl}$ ($n = 9$) or *Piezo1*$^{\Delta LysM}$ ($n = 9$) lungs infected intranasally with *P. aeruginosa* for 6 h. Data are from two independent experiments. **e**, ELISA quantification of indicated cytokines and PGE2 from BALF of *Piezo1*$^{fl/fl}$ and *Piezo1*$^{\Delta LysM}$ mice infected intranasally with *P. aeruginosa* for 2 h. Data are presented as three biological replicates from two independent experiments. **f**, Mean fluorescent intensity (MFI) of HIF1α from total lung interstitial monocytes of *Piezo1*$^{fl/fl}$ ($n = 7$) and *Piezo1*$^{\Delta LysM}$ ($n = 6$) mice infected intranasally with *P. aeruginosa* for 6 h. Data are from two independent experiments. AU, arbitrary units. **g**, Quantification of EDN1 by ELISA from BALF of *Piezo1*$^{fl/fl}$, *Piezo1*$^{\Delta LysM}$ or *Piezo1*$^{\Delta CD11c}$ mice infected intranasally with *P. aeruginosa* for 2 h. Data are presented as six (*Piezo1*$^{fl/fl}$) or three (*Piezo1*$^{\Delta LysM}$ and *Piezo1*$^{\Delta CD11c}$) biological replicates. **h**, ELISA quantification of EDN1 and CXCL2 from BALF of mice depleted of monocytes with intraperitoneal CCR2 antibody (20 μg) or with isotype control 24 h before infection. Data are presented as four biological replicates. **i**, *P. aeruginosa* counts from lung of *Piezo1*$^{fl/fl}$ mice, pre-treated with 25 μg EDN1-blocking antibody ($n = 5$) or isotype control ($n = 6$) intranasally 6 h before infection. Data are from two independent experiments. Dotted line, limit of detection. **j**, *P. aeruginosa* counts from lung of *Piezo1*$^{\Delta LysM}$ mice infected intranasally with *P. aeruginosa* for 24 h, treated with vehicle (PBS) ($n = 10$) or 10 μg rEDN1 ($n = 9$) intranasally at the time of infection. Data are from two independent experiments. Dotted line, limit of detection. **k**, ELISA quantification of EDN1 from BALF 14 days after intratracheal bleomycin treatment of *Piezo1*$^{fl/fl}$ ($n = 7$) or *Piezo1*$^{\Delta LysM}$ ($n = 8$) mice. Data are representative of two independent experiments. **l**, Representative haematoxylin and eosin staining of lung sections 14 days after intratracheal bleomycin treatment. Original magnification, 10×. Data are representative of two independent experiments. **m**, Average blinded Ashcroft score of five fields of view from fixed lung tissue of *Piezo1*$^{fl/fl}$ ($n = 7$) or *Piezo1*$^{\Delta LysM}$ ($n = 8$) mice 14 days following intratracheal bleomycin treatment, with haematoxylin and eosin staining. Data are representative of two independent experiments. Data in **a**, **b**, **i**, **j**, are mean ± s.e.m.; significance is determined by two-tailed Mann–Whitney *U*-test (**$P < 0.01$ and ***$P < 0.001$). Data in **c**-**h**,**k**,**m** are mean ± s.e.m.; significance is determined by unpaired two-tailed Student's *t*-test (*$P < 0.05$, **$P < 0.01$, ***$P < 0.001$ and ****$P < 0.0001$).

of CHP-induced transcriptional reprogramming (Fig. 2l). However, guide RNAs targeting the B-cell-specific protein CD79a and endothelin receptor A (*Ednra*), which are not expressed in macrophages, had no effect on CHP-mediated transcriptional reprogramming, indicating that Cas9-mediated activity itself does not affect the pathway (Fig. 2l). These results identify a PIEZO1-dependent mechanism of early AP-1 activation in response to CHP that drives transcription of *Edn1*. EDN1 signalling triggers HIF1α stabilization, facilitating prolonged proinflammatory cytokine expression. Together, these results delineate a circuit that links mechanosensation to innate immunity.

CHP drives inflammation via PIEZO1 and EDN1

Next, we sought to determine whether PIEZO1 was required for host defence during a physiological bacterial infection. As cells in the lung experience high amounts of mechanostimulation[8], and as *Pseudomonas aeruginosa* infection results in an altered pulmonary mechanoenvironment[30], we chose this model to investigate the physiological role of PIEZO1 in innate immunity. We detected high levels of PIEZO1 in myeloid cells isolated from the lung (Extended Data Fig. 5a–c). We infected *Piezo1*$^{fl/fl}$ and *Piezo1*$^{\Delta LysM}$ mice with 5×10^6 colony-forming units (CFU) of *P. aeruginosa* intranasally. After 24 h, *Piezo1*$^{\Delta LysM}$ mice had higher bacterial loads in lung and liver than *Piezo1*$^{fl/fl}$ littermates, suggesting an inability to control bacterial infection and prevent systemic dissemination (Fig. 3a, b). We next tested for differences in pulmonary immune-cell recruitment at early time points of infection. Because the lung is a highly vascularized organ, we used in vivo labelling with CD45.2 antibody to separate immune cells in circulation from infiltrated or tissue-protected immune cells[31]. We observed decreased numbers of tissue-infiltrating neutrophils in *Piezo1*$^{\Delta LysM}$ mice 6 h after infection compared to *Piezo1*$^{fl/fl}$ mice, but no difference in monocyte levels. (Fig. 3c, d, Extended Data Fig. 6a–c). Two hours after infection, *Piezo1*$^{\Delta LysM}$ bronchoalveolar lavage fluid (BALF) contained significantly decreased levels of inflammatory mediators previously shown to be PIEZO1-inducible in monocytes and BMDMs in vitro compared to *Piezo1*$^{fl/fl}$ mice (Fig. 3e).

To investigate whether this heightened proinflammatory response was a result of increased HIF1α, we infected *Piezo1*$^{fl/fl}$ and *Piezo1*$^{\Delta LysM}$ mice with *P. aeruginosa* for 6 h and analysed intracellular HIF1α levels in lung immune cells. Only infiltrated monocytes showed robust upregulation of HIF1α, which was dependent on PIEZO1 (Fig. 3f, Extended Data Fig. 6d). Circulating monocytes showed no HIF1α accumulation (Extended Data Fig. 6e). As previous reports have described that extravasation alone can result in immune-cell activation in vitro[7], the observed HIF1α stabilization could conceivably be triggered by force exerted on monocytes during extravasation or by the hydrostatic pressure microenvironment encountered by monocytes during pulmonary recruitment. To test this, we infected mice with *P. aeruginosa* intraperitoneally, and observed no upregulation of HIF1α in peritoneal-recruited monocytes (Extended Data Fig. 6f).

This observation demonstrates that the shear stress provoked by extravasation is insufficient on its own to stabilize HIF1α in monocytes. Furthermore, macrophages subjected to oscillatory shear stress in vitro upregulated *Icam1*(Extended Data Fig. 6g), an important molecule for cellular adhesion that has been shown to be regulated by shear force[7]. However, *Icam1* upregulation was independent of PIEZO1 (Extended Data Fig. 6g). Notably, as oscillatory shear stress did not upregulate the PIEZO1-dependent program of proinflammatory genes (Extended Data Fig. 6g), we conclude that the specific mechanism of this response involves CHP and HIF1α stabilization. We next tested whether PIEZO1-dependent EDN1 production has a critical role in antibacterial defence in vivo. Although *P. aeruginosa* infection triggered EDN1 in BALF 2 h after infection in $Piezo1^{fl/fl}$ mice, EDN1 was not detected in cells from $Piezo1^{\Delta LysM}$ mice (Fig. 3g). To test whether alveolar macrophages were the major source of EDN1, we crossed $Piezo1^{fl/fl}$ mice with *CD11c-Cre* mice, resulting in deletion of PIEZO1 in alveolar macrophages and dendritic cells[32]. $Piezo1^{\Delta CD11c}$ mice showed no reduction in EDN1 levels in BALF 2 h after infection with *P. aeruginosa*, implying that PIEZO1 has no role in EDN1 expression from alveolar macrophages or dendritic cells (Fig. 3g). Therefore, as neutrophils do not express PIEZO1 (Extended Data Fig. 5c), we hypothesized that monocytes are likely to have a critical role in PIEZO1-mediated upregulation of EDN1 expression. To test this possibility, we administered a monoclonal antibody against CCR2 that has been shown to deplete monocytes efficiently[33]. Monocyte depletion resulted in significant loss of EDN1 from the BALF compared to isotype control 6 h after bacterial infection (Fig. 3h). Furthermore, we also identified monocytes as a major cellular source of the neutrophil chemoattractant CXCL2 (Fig. 3h), another CHP-inducible gene (Fig. 1b). Next, we tested whether EDN1 was required for *P. aeruginosa* clearance. Mice administered with EDN1-blocking antibody showed increased levels of bacterial abundance in the lung and liver 24 h after *P. aeruginosa* infection compared to isotype control (Fig. 3i, Extended Data Fig. 7a). To test whether EDN1 could rescue $Piezo1^{\Delta LysM}$ mice, we administered recombinant EDN1 intranasally, and observed decreased levels of bacteria in lung and liver 24 h after infection compared to vehicle-treated mice (Fig. 3j, Extended Data Fig. 7b). Treatment with bosentan also resulted in susceptibility to bacterial infection (Extended Data Fig. 7c, d). Thus, PIEZO1 is essential for myeloid-cell-mediated protection from *P. aeruginosa* and vital for EDN1 production and HIF1α activation in newly recruited monocytes, which in turn drive neutrophil recruitment and pathogen clearance.

Given its importance in pathogen-induced inflammation, we sought to investigate whether PIEZO1-mediated myeloid-cell activation could also drive autoinflammatory disease associated with mechanical perturbations in the lung. Bleomycin-induced pulmonary fibrosis results in aberrant alterations of the lung mechanical environment[34]. We observed reduced levels of EDN1 from BALF and protection from bleomycin-induced lung damage in $Piezo1^{\Delta LysM}$ mice as measured by Ashcroft scoring[35] (Fig. 3k–m). Therefore, PIEZO1 is not only relevant in pulmonary infection but also has a physiologically important role in driving pathology during autoinflammatory processes such as pulmonary fibrosis.

Discussion

Here we identify a mechanism that enables myeloid cells to sense their physical environment and integrate this information with other signals to generate a selective innate immune response. Specifically, PIEZO1 signalling drives myeloid cells towards a proinflammatory expression profile dependent on AP-1 activation, EDN1 expression and HIF1α stabilization (Extended Data Fig. 8). Physiologically, we demonstrate that PIEZO1-mediated mechanosensation is essential for protection against bacterial infection in the lung and can drive robust pathological tissue damage during pulmonary fibrosis. We find that infiltrating lung monocytes respond to CHP by stabilizing HIF1α and secreting molecules such as EDN1 and the neutrophil chemoattractant CXCL2 (Extended Data Fig. 9). These findings indicate that immune-cell recognition of force and pressure is not only an important cue for an appropriate immune response to pulmonary infection, but can also perpetuate and exacerbate pathogenic autoinflammation in the context of pulmonary fibrosis. This understanding of how force and pressure affect the immune response may lead to novel mechanistic insights into disease progression and, ultimately, to new avenues in therapeutic treatment.

Whereas newly recruited monocytes use PIEZO1 to drive HIF1α-stabilization and instigate a proinflammatory state during pulmonary infection, alveolar macrophages do not appear to activate this PIEZO1-dependent pathway in response to pulmonary CHP. As alveolar macrophages spend their entire lifecycle subjected to CHP in the lung, the PIEZO1 ion channel is likely to become desensitized in this population in response to prolonged mechanical stimulation, to prevent chronic inflammation—as is the case for this channel in other cell types[36]. Conversely, it is also possible that PIEZO1 signalling in alveolar macrophages is functional but specifies a distinct mechanistic contribution to pulmonary homeostasis or immunity that is not detected in this study. Further investigation is necessary to delineate a role of PIEZO1 in alveolar macrophages and other immune cell types in the lung.

Our work highlights force as a novel parameter of immune-cell activation and reveals an unexpected complexity in myeloid-cell mechanosensation. Specifically, cyclical pressure and shear stress initiate non-overlapping signalling consequences in myeloid cells, resulting in a tailored response to the physiologically distinct mechanical stimulations. For example, in vitro modelling of the shear stress forces experienced during the process of extravasation drives upregulation of *Icam1* in a process entirely independent of PIEZO1. Therefore, recognition of the mechanical response to oscillatory shear stress is initiated by distinct mechanical sensors, and presumably effectors, to those used during CHP detection. In addition to MSICs, other proteins have been demonstrated to recognize mechanical stimulation[6]. One potential candidate for the sensor of oscillatory shear stress is focal adhesion kinase, which is expressed in macrophages[37] and has been shown to respond to shear forces[38]. Identification of the sensors and effectors of different forms of immune-cell mechanosensation will be essential to complete our understanding of complex immunological disease.

Finally, whereas our studies have initially focused solely on immune responses in the pulmonary CHP microenvironment, how immune cells recognize and respond to force in other mucosal and non-mucosal tissues remians unknown. For example, the intestine is a site of constant rhythmic mechanical stimulation in the form of peristalsis, which can dynamically and markedly change during enteric infection and autoinflammatory conditions such as inflammatory bowel disease[39]. Further work will be required to investigate whether immune-cell PIEZO1 signalling or other sensors of mechanosensation contribute to intestinal inflammation and disease.

In sum, our work shows that mechanical stimulation alone, even in the absence of classical PRR signalling, results in innate immune activation. This work identifies force as a parameter that alters immune-cell function, and is probably relevant in other cells, organs, diseases and immunological processes.

Online content

Any methods, additional references, Nature Research reporting summaries, source data, extended data, supplementary information, acknowledgements, peer review information; details of author contributions and competing interests; and statements of data and code availability are available at https://doi.org/10.1038/s41586-019-1485-8.

Received: 16 November 2018; Accepted: 16 July 2019;
Published online 21 August 2019.

1. Pritchard, M. T., Li, Z. & Repasky, E. A. Nitric oxide production is regulated by fever-range thermal stimulation of murine macrophages. *J. Leukoc. Biol.* **78**, 630–638 (2005).
2. Anand, R. J. et al. Hypoxia causes an increase in phagocytosis by macrophages in a HIF-1α-dependent manner. *J. Leukoc. Biol.* **82**, 1257–1265 (2007).

3. Ip, W. K. E. & Medzhitov, R. Macrophages monitor tissue osmolarity and induce inflammatory response through NLRP3 and NLRC4 inflammasome activation. *Nat. Commun.* **6**, 6931 (2015).
4. Littlewood-Evans, A. et al. GPR91 senses extracellular succinate released from inflammatory macrophages and exacerbates rheumatoid arthritis. *J. Exp. Med.* **213**, 1655–1662 (2016).
5. Palm, N. W. & Medzhitov, R. Pattern recognition receptors and control of adaptive immunity. *Immunol. Rev.* **227**, 221–233 (2009).
6. Huse, M. Mechanical forces in the immune system. *Nat. Rev. Immunol.* **17**, 679–690 (2017).
7. Hsiai, T. K. et al. Monocyte recruitment to endothelial cells in response to oscillatory shear stress. *FASEB J.* **17**, 1648–1657 (2003).
8. McWhorter, F. Y., Davis, C. T. & Liu, W. F. Physical and mechanical regulation of macrophage phenotype and function. *Cell. Mol. Life Sci.* **72**, 1303–1316 (2015).
9. Coste, B. et al. Piezo1 and Piezo2 are essential components of distinct mechanically activated cation channels. *Science* **330**, 55–60 (2010).
10. Murthy, S. E. et al. The mechanosensitive ion channel Piezo2 mediates sensitivity to mechanical pain in mice. *Sci. Transl. Med.* **10**, eaat9897 (2018).
11. Gudipaty, S. A. et al. Mechanical stretch triggers rapid epithelial cell division through Piezo1. *Nature* **543**, 118–121 (2017).
12. Wang, S. et al. Endothelial cation channel PIEZO1 controls blood pressure by mediating flow-induced ATP release. *J. Clin. Invest.* **126**, 4527–4536 (2016).
13. Delmas, P., Hao, J. & Rodat-Despoix, L. Molecular mechanisms of mechanotransduction in mammalian sensory neurons. *Nat. Rev. Neurosci.* **12**, 139–153 (2011).
14. Schipke, K. J., To, S. D. F. & Warnock, J. N. Design of a cyclic pressure bioreactor for the ex vivo study of aortic heart valves. *J. Vis. Exp.* (54):3316 (2011).
15. Li, J. et al. Piezo1 integration of vascular architecture with physiological force. *Nature* **515**, 279–282 (2014).
16. He, Y., Hara, H. & Núñez, G. Mechanism and regulation of NLRP3 inflammasome activation. *Trends Biochem. Sci.* **41**, 1012–1021 (2016).
17. Tannahill, G. M. et al. Succinate is an inflammatory signal that induces IL-1β through HIF-1α. *Nature* **496**, 238–242 (2013).
18. Yamashita, K., Discher, D. J., Hu, J., Bishopric, N. H. & Webster, K. A. Molecular regulation of the endothelin-1 gene by hypoxia. Contributions of hypoxia-inducible factor-1, activator protein-1, GATA-2, and p300/CBP. *J. Biol. Chem.* **276**, 12645–12653 (2001).
19. Lee, J. J. et al. Hypoxia activates the cyclooxygenase-2-prostaglandin E synthase axis. *Carcinogenesis* **31**, 427–434 (2010).
20. Palazon, A., Goldrath, A. W., Nizet, V. & Johnson, R. S. HIF transcription factors, inflammation, and immunity. *Immunity* **41**, 518–528 (2014).
21. Varia, M. A. et al. Pimonidazole: a novel hypoxia marker for complementary study of tumor hypoxia and cell proliferation in cervical carcinoma. *Gynecol. Oncol.* **71**, 270–277 (1998).
22. Mekhail, K., Gunaratnam, L., Bonicalzi, M.-E. & Lee, S. HIF activation by pH-dependent nucleolar sequestration of VHL. *Nat. Cell Biol.* **6**, 642–647 (2004).
23. Glogowska, E. et al. Novel mechanisms of PIEZO1 dysfunction in hereditary xerocytosis. *Blood* **130**, 1845–1856 (2017).
24. Miyamoto, T. et al. Functional role for Piezo1 in stretch-evoked Ca^{2+} influx and ATP release in urothelial cell cultures. *J. Biol. Chem.* **289**, 16565–16575 (2014).
25. Stow, L. R., Jacobs, M. E., Wingo, C. S. & Cain, B. D. Endothelin-1 gene regulation. *FASEB J.* **25**, 16–28 (2011).
26. Li, M. et al. Endothelin-1 induces hypoxia inducible factor 1α expression in pulmonary artery smooth muscle cells. *FEBS Lett.* **586**, 3888–3893 (2012).
27. Liu, Y. V. et al. Calcineurin promotes hypoxia-inducible factor 1α expression by dephosphorylating RACK1 and blocking RACK1 dimerization. *J. Biol. Chem.* **282**, 37064–37073 (2007).
28. Cheng, T.-H. et al. Reactive oxygen species mediate cyclic strain-induced endothelin-1 gene expression via Ras/Raf/extracellular signal-regulated kinase pathway in endothelial cells. *J. Mol. Cell. Cardiol.* **33**, 1805–1814 (2001).
29. Bailis, W. et al. Distinct modes of mitochondrial metabolism uncouple T cell differentiation and function. *Nature* **571**, 403–407 (2019).
30. Lindsey, A. S. et al. Analysis of pulmonary vascular injury and repair during *Pseudomonas aeruginosa* infection-induced pneumonia and acute respiratory distress syndrome. *Pulm. Circ.* **9**, 1–13 (2019).
31. Novak, J., Georgakoudi, I., Wei, X., Prossin, A. & Lin, C. P. In vivo flow cytometer for real-time detection and quantification of circulating cells. *Opt. Lett.* **29**, 77–79 (2004).
32. Abram, C. L., Roberge, G. L., Hu, Y. & Lowell, C. A. Comparative analysis of the efficiency and specificity of myeloid-Cre deleting strains using ROSA-EYFP reporter mice. *J. Immunol. Methods* **408**, 89–100 (2014).
33. Mack, M. et al. Expression and characterization of the chemokine receptors CCR2 and CCR5 in mice. *J. Immunol.* **166**, 4697–4704 (2001).
34. Phillips, J. E. et al. Bleomycin induced lung fibrosis increases work of breathing in the mouse. *Pulm. Pharmacol. Ther.* **25**, 281–285 (2012).
35. Ashcroft, T., Simpson, J. M. & Timbrell, V. Simple method of estimating severity of pulmonary fibrosis on a numerical scale. *J. Clin. Pathol.* **41**, 467–470 (1988).
36. Wu, J. et al. Inactivation of mechanically activated Piezo1 ion channels is determined by the C-terminal extracellular domain and the inner pore helix. *Cell Rep.* **21**, 2357–2366 (2017).
37. Abshire, M. Y., Thomas, K. S., Owen, K. A. & Bouton, A. H. Macrophage motility requires distinct α5β1/FAK and α4β1/paxillin signaling events. *J. Leukoc. Biol.* **89**, 251–257 (2011).
38. Young, S. R. L., Gerard-O'Riley, R., Kim, J.-B. & Pavalko, F. M. Focal adhesion kinase is important for fluid shear stress-induced mechanotransduction in osteoblasts. *J. Bone Miner. Res.* **24**, 411–424 (2009).
39. Bassotti, G. et al. Gastrointestinal motility disorders in inflammatory bowel diseases. *World J. Gastroenterol.* **20**, 37–44 (2014).
40. Rajamäki, K. et al. Extracellular acidosis is a novel danger signal alerting innate immunity via the NLRP3 inflammasome. *J. Biol. Chem.* **288**, 13410–13419 (2013).

METHODS

Animals. *Piezo1*$^{fl/fl}$ mouse embryonic stem cells were obtained from the KnockOut Mouse Project Repository. Embryonic stem cells were injected into a blastocyst, and the F1 generation were backcrossed to C57Bl/6 mice to obtain homozygous-floxed mice. Mice were then crossed to LysM-Cre mice obtained from Jackson Laboratories. Experimental groups of mice were obtained by crossing homozygous *Piezo1*$^{fl/fl}$; homozygous Cre-negative to homozygous *Piezo1*$^{fl/fl}$; heterozygous Cre-positive mice, which would theoretically produce an equal number of Cre-negative and Cre-positive mice. All experiments were performed using littermate control, cohoused mice. All animal experimentation was performed in compliance with Yale Institutional Animal Care and Use Committee protocols.

Generation of BMDMs. Mice were euthanized and hind legs were removed and placed in conical tubes containing 5% FCS DMEM medium (Gibco). Muscle was removed from tibia and femur bones and the ends of bones were cut off. Using a 27½ gauge needle, 10 ml of sterile DMEM supplemented with 10% FBS, penicillin–streptomycin and L-glutamine was passed through the bone. Cells were pelleted and plated with mouse MCSF (50 ng ml^{-1}) (BioLegend). Following 4 days of incubation, supernatant was removed and plated in a new dish. Cells were again incubated in medium with mouse MCSF for 3 more days. Dishes were then washed 3 times with sterile PBS to remove unadhered cells. BMDMs were gently scraped off the dish, pelleted, counted, and seeded in new plates for experimentation. In the case of experiments with calcium-free medium, immediately before experimentation, cells were washed three times with PBS before adding calcium-free DMEM with penicillin–streptomycin and L-glutamine. Controls for a calcium-free medium experiment were placed in calcium-sufficient DMEM with penicillin–streptomycin and L-glutamine.

RNA isolation and processing. BMDMs were plated at 1×10^6 to 2×10^6 cells per well on a flat bottom non-adherent 12-well plates. Following treatment, cells were washed once with PBS, and gently dislodged from the plate with PBS. Cells were pelleted and then processed using Qiagen RNeasy Mini Plus Kit (Qiagen) using the manufacturer's protocol. RNA quantity was assayed using a NanoDrop Microvolume Spectrophotometer (Thermo). RNA was sent for RNA-sequencing or converted to cDNA using Maxima H Minus Reverse Transcriptase Kit and using the manufacturer's protocol (Thermo). qPCR was conducted using Sigma KiCqStart predesigned SYBR green primers and iTaq Universal SYBR Green Supermix (Bio-Rad). Relative mRNA amounts were compared to *Gapdh* mRNA levels. mRNA for RNA-seq analysis was purified using polyA$^+$ selection and processed by the Yale Center for Genome Analysis using standard methodology and sequenced on a HiSeq2000 with 75-bp pair-ended reads.

Pressure chamber. All pressure chamber experiments used a custom-built pressure chamber bioreactor built at the laboratory of J.N.W. The chamber computational board was connected to a laptop running custom software designed and coded on LabVIEW. The air-intake valve was connected to a regulated gas tank containing 5% CO_2 balanced in air (21% O_2 and 79% N_2), except in the case of hypoxia-synergy studies, in which a gas tank containing 2% O_2, rather than 21% O_2, was substituted. The chamber was placed inside a tissue culture chamber to allow temperatures to reach 37 °C. The program parameters were set such that the air intake valve would be open for 0.6 s, then the exhaust valve would be opened for 0.4 s at a sampling rate of 10 samples per second. The regulator on the gas tank was adjusted such that the amplitude of cyclical hydrostatic pressure was approximately 15 mmHg, and adjustments were made constantly throughout the experiments to maintain this amplitude. For static pressure control experiments, both the air intake and exhaust valve were opened, and the regulator was adjusted such that the pressure within the chamber reached the lower parameter achieved in the corresponding cyclical hydrostatic pressure experiment, unless otherwise noted.

RNA-seq analysis. Fragments were mapped to the mouse genome (mm9) with Tophat2 using default parameters. A reference transcriptome consisting of UCSC known genes was used for isoform-level quantification and differential analysis using Cuffdiff2. Quality control analysis and visualization were done using the CummeRbund package, which is part of the R/Bioconductor suite of utilities. Differentially expressed genes between samples were selected with a Benjamini–Hochberg corrected P value <0.05 deemed by the Cuffdiff2 program as significant. Volcano plots were generated using Prism and Heat maps were generating using Morpheus by Broad Institute.

ELISA. Treated and nontreated BMDM supernatants were centrifuged at 13,000*g* for 10 min to remove cellular debris. ELISA measurements were conducted using kits for CXCL10, EDN1, IL-1β (R&D DuoSets) or PGE2 (R&D Parameter Assay).

Western blotting. Treated and nontreated BMDMs were washed on ice with ice cold PBS, then lysed over 30 min with ice-cold RIPA Lysis Buffer containing a cocktail of protease inhibitors (Roche) and phosphatase inhibitors (NEB) with gentle agitation every 10 min. Cellular debris was clarified (13,000*g*, 10 min, 4 °C). Reducing agent (NuPAGE Thermo) and sample buffer was added to supernatant, and boiled at 95 °C for 10 min. Protein lysates were resolved on NuPAGE 4–12% Bis-Tris Protein Gels using MOPS running buffer (Invitrogen), transferred to nitrocellulose membrane and blocked with 5% OmniBlok Dry Milk in PBS. Detection of HIF1α (D2U3T), Hif2α (D9E3), phospho- JUN (54B3 and 9164), phospho-JNK (81E11), total JUN (60A8) and total JNK (9252) was done using monoclonal antibodies (Cell Signaling). β-tubulin (E7) was detected using a monoclonal antibody (DSHB). HRP-conjugated anti-rabbit (Cell Signaling, 7074) or anti-mouse antibody (GE Healthcare, NA931V) was used as secondary antibodies and detected using SuperSignal West Pico PLUS Chemiluminiscent Substrate (Thermo) and autoradiography film (Denville).

Confocal microscopy. For HIF1α detection, BMDMs were fixed with 4% methanol-free paraformaldehyde for 10 min and permeablized with 0.3% Triton X for 30 min. Cells were blocked with 2% BSA 0.1% Triton X-100 and stained with a monoclonal Rabbit anti-HIF1α antibody (Cell Signaling, D1S7W). Cells were then washed, stained with a polyclonal anti-rabbit secondary (Life Technologies), and imaged with a Nikon-Ti microscope combined with UltraVox spinning disk (PerkinElmer) and data were analysed using the Volocity software (PerkinElmer).

Intracellular pH assay. Intracellular pH was measured using cell-permeable pHrodo red AM intracellular pH sensor (Invitrogen). Macrophages were subjected to cyclical hydrostatic pressure. In the final 30 min of mechanostimulation, cells were washed according to the manufacturer's protocol and pHrodo dye was added. As a control, cells were incubated in the absence of mechanostimulation in acidic DMEM (pH 6.5). Cells were then washed again on ice and immediately analysed via flow cytometry.

Oscillatory shear stress. Macrophages were plated on plastic slides coated with fibronectin (20 μg ml^{-1}) for two days. The slides were mounted into parallel-plate flow chambers and subjected to oscillatory flow (1 ± 5 dynes cm^{-2}, 1 Hz) for 6 h. Flow was applied using a syringe pump (NE1050, New Era Pump Systems) combined with a peristaltic pump (Masterflex C/L, Cole Palmer) for medium circulation. Medium was maintained at 37 °C using a temperature control system (Cole Palmer) and infused with 5% CO_2.

sgRNA cloning and retroviral production. MGguide was modified to contain an *Escherichia coli* phenylalanyl-tRNA synthetase a-subunit (ePheS) negative selection cassette and to express human NGFR (Addgene) under control of the SV40 promoter. To clone individual sgRNAs, the vector was digested with BbsI, eliminating the ePheS cassette, and annealed oligonucleotides with complementary overhangs were ligated into the vector using T4 DNA ligase (NEB). STBL3 cells (Invitrogen) were transformed and grown on plates and in medium containing 16 mM 4-Chloro-DL-phenylalanine (Alfa Aesar) and Ampicillin. For retroviral production, 7E6 293T cells were plated in a 10-cm dish and the following day were transfected with 5.3 μg of MG-guide and 2.6 μg of EcoHelper plasmid (Addgene) using LipoD293 transfection reagent. At 24 h medium was replaced, and at 48 h supernatants were collected.

CRISPR knockout. CRISPR–Cas9-knockout experiments were carried out using a modified version of a previously published protocol. In brief, bone marrow from Cas9-transgenic mice was collected and cultured in complete DMEM with MCSF (50 ng ml^{-1}) in non-tissue culture treated dishes. Twenty-four hours later, medium was replaced with MG-guide retroviral supernatants supplemented with MCSF. Three days later, BMDMs were detached using Accutase (Sigma # A6964-100ML) and live CD11b-positive cells were FACS sort purified based on hNGFR reporter expression using the following reagents: biotin-labelled anti-human CD271 (BD biosciences), BV421-labelled streptavidin (Biolegend), BV711 labelled CD11b antibody (Biolegend), Fixable Viability Dye eFluor 780 (ThermoFisher). Sorted cells were plated in 24-well plates at 5×10^5 cells per ml in medium containing MCSF.

P aeruginosa infection. *P. aeruginosa* (PA14 strain provided by B. Kaczmierczek, Yale University) was maintained as a glycerol stock at −80 °C. One day before infection, bacteria were grown at 37 °C in a shaking incubator for approximately 16 h in LB medium. Bacteria were subcultured in a 1:20 ratio in a volume of 20mL until OD600 was between 1.5 and 2.0, which is approximately 1.5×10^9 and 2×10^9 CFU ml^{-1}. A dose of 2.5×10^8 CFU was diluted in 1ml sterile PBS, washed twice (8,000 r.p.m., 2 min), and diluted to a final volume of 1ml. Mice were anesthetized with methoxyflurane, and a dose of 5×10^6 CFU was instilled intranasally using a micropipette.

In vivo labelling of CD45.2$^+$ cells. Mice were anesthetized using isoflurane and intravenously injected with 100 μl PBS containing CD45.2-Pacific Blue antibody (Biolegend, clone 104, 1:40 dilution). After 5 min, mice were then sacrificed and samples were collected for flow cytometry as described below.

Lung processing and flow cytometry. Mice were euthanized and lungs were removed and placed in fresh medium on ice. Tissues were then finely chopped with clean dissection scissors, and digested with medium containing collagenase D (1 mg ml^{-1}) (Sigma) and DNase I (Sigma) for 30–60 min. Cells were then filtered through a 70 μm filter and pelleted. Epithelial cells were removed using an 80% to 40% Percoll gradient (GE Healthcare) spun at 600*g* for 20 min with slow acceleration and no brake at room temperature. Cells between the gradient were removed and pelleted. Red blood cells were lysed using ACK Lysis Buffer (Vita Scientific). Cells were then stained for 30 min at 4 °C in the dark using the following Biolegend

antibodies: CD45.2 (clone 104), TCRβ (clone H97-597), TCR γ/δ (clone GL3), NK1.1 (clone PK136), B220 (clone RA3-6B2), CD19 (clone 6D5), Ly6c (clone HK1.4), Ly6g (clone 1A8), CD169 (clone 3D6.112), Ter119 (clone Ly-76), CD90.2 (clone 53-2.1), CD11c (clone N418), SiglecF (R&D BAF1706) and CD11b (clone M1/70). For intracellular staining, cells were fixed and permeablized using the Foxp3/Transcription Factor Staining Buffer Set (eBioscience) exactly as described in the manufacturer's protocol. Intracellular HIF1α was probed using a monoclonal PE-conjugated antibody (CST, D1S7W). Cells were then filtered through a 40-μm filter, and 20,000 counting beads (Invitrogen) were added. Samples were resuspended in PBS containing 2% FCS and 2mM EDTA and acquired with an LSRII cytometer (BD Bioscience) and analysed using FlowJo (BD Bioscience).

Bronchoalveolar lavage fluid molecular measurement. Mice were euthanized and the trachea was exposed surgically. A small incision was made into the trachea to allow a blunt-ended needle to be inserted and tied with sutures. Lungs were aspirated with 1 ml sterile PBS and placed in a 2-ml microcentrifuge tube on ice. Cells and cellular debris was removed by centrifugation (12,000*g*, 10 min, 4 °C) and supernatants were analysed for IL-6, IL-10, TNF, IL-33, IL-4, CXCL2 (R&D Duoset) and PGE2 (R&D Parameter Assay).

Hypoxia studies. Differentiated BMDMs were plated in glass bottom 24-well plates and incubated for 6 h either in static pressure, cyclic pressure or in a hypoxia chamber (2% O_2, 5% CO_2, N_2). After 6 h, cells were analysed for transcriptional profile as described above. Pimonidazole (20 μM, Hypoxyprobe) was added in the last hour of incubation, and cells were then fixed and permeablized using the Foxp3/Transcription Factor Staining Buffer Kit (eBioscience). Pimonidazole was detected using a monoclonal antibody conjugated to Cy7-conjugated (1:200, Hypoxyprobe). Confocal microscopy was conducted as described above.

Pulmonary fibrosis. Lung fibrosis model was established using bleomycin (Zydus Hospira Oncology). In brief, mice were anesthetized using 3% isoflurane and instilled with 1.5 U per kg (body weight) of bleomycin in 50 μl PBS by intratracheal route using oropharyngeal aspiration. Mice were euthanized at 14 days after bleomycin, at which time there were obvious fibrotic changes in the lung.

Reporting summary. Further information on research design is available in the Nature Research Reporting Summary linked to this paper.

Data availability

The authors declare that all data supporting the findings of this study are available within this article and its Supplementary Information files. RNA-sequencing data have been deposited in the Gene Expression Omnibus database under the accession code GSE133069.

Acknowledgements We thank J. Alderman, C. Lieber, C. Hughes, E. H.-P. and P. Rainey for help in facilitating this work; B. Kazmierczak for providing the *P. aeruginosa*; M. Roulis for insightful comments and reagents; L. Orr for helpful insight regarding statistical analysis; I. Odell for help with computational software; C. Rothlin and Dr. C. Abraham for continued support and feedback as this work progressed; P.-M. Chen for help and reagents related to hypoxia studies. This work was supported by the Howard Hughes Medical Institute and the Blavatnik Family Foundation (R.A.F.). This work was supported in part by the Searle Scholars Program, the Leukemia Research Foundation, the Gruber Foundation and the NIH (R01GM122984). R.J. was supported in part by the Crohn's and Colitis Foundation. M.A.S. was supported by the NIH (HL RO1 75092). A.G.S. was supported in part by an NIH training grant (T32 GM007499) and the American Society for Microbiology.

Author contributions A.G.S. designed and performed experiments, collected and analysed data, and wrote the manuscript. P.B. performed microbiological experiments and offered vital conceptual insight. H.R.S. developed reagents and performed Cas9 experiments. L.S. performed in vivo fibrosis experiments. C.C.D.H. performed all bioinformatic analysis. S.Y. performed in vitro shear stress experiments. M.R.d.Z. offered conceptual insight. J.N.W. and S.D.F.T. designed and built the bioreactor and software necessary to complete mechanistic experiments. A.G.Y. helped collect samples. M.M. provided critical reagents and advice on experimental design. M.A.S. and C.S.D.C. provided intellectual support and resources. N.W.P. originally proposed the study. R.J. and R.A.F supervised the project, helped interpret the work and supervised writing of the manuscript.

Competing interests : R.A.F. is a scientific advisor to GlaxoSmithKline, a consultant for Hatteras Venture Partners and a shareholder and consultant for Zai Lab Ltd. All other authors declare no competing interests.

Additional information
Supplementary information is available for this paper at https://doi.org/10.1038/s41586-019-1485-8.
Correspondence and requests for materials should be addressed to R.J. or R.A.F.
Peer review information *Nature* thanks Seth Alper, Luke O'Neill, Sarah Walmsley and the other, anonymous, reviewer(s) for their contribution to the peer review of this work.
Reprints and permissions information is available at http://www.nature.com/reprints.

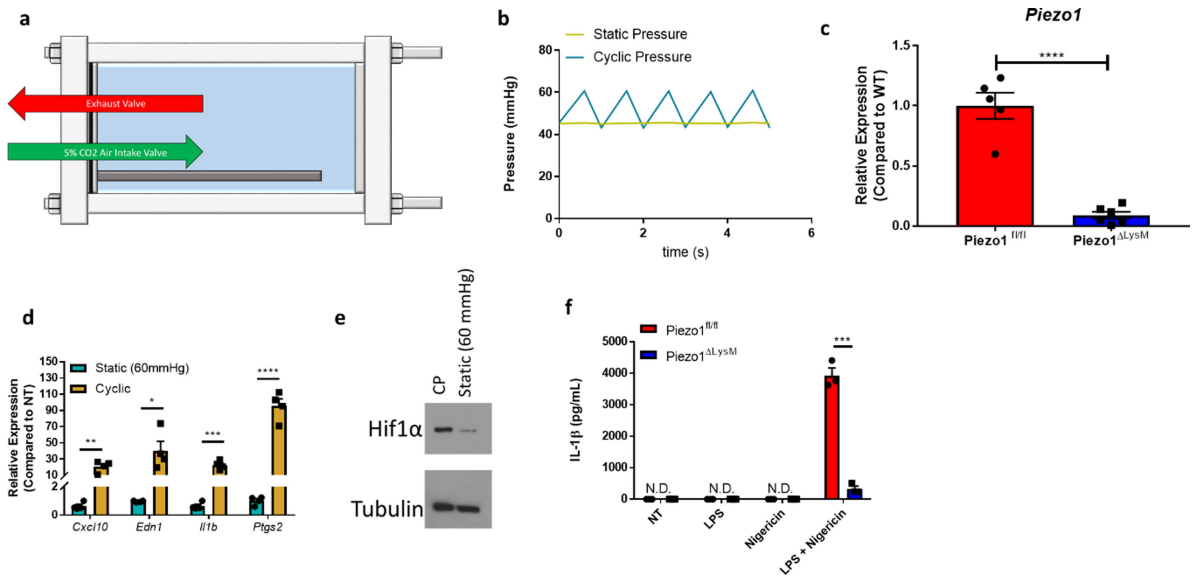

Extended Data Fig. 1 | Pressure chamber schematic and PIEZO1-knockout validation. a, Schematic of CHP bioreactor showing side view. **b**, Graph of pressure regimes used within the pressure chamber. **c**, RT–qPCR analysis of *Piezo1* in unstimulated BMDMs from *Piezo1*$^{fl/fl}$ (WT) and *Piezo1*$^{\Delta LysM}$ mice. Data are presented as five biological replicates from two independent experiments. **d**, RT–qPCR analysis of *Piezo1*$^{fl/fl}$ BMDMs treated with static pressure at the indicated magnitude or with CHP for 6 h. Data are presented as four biological replicates from two independent experiments. **e**, Immunoblot analysis of HIF1α and β-tubulin from *Piezo1*$^{fl/fl}$ BMDMs treated with static pressure at the indicated magnitude or with CHP for 6 h. Data are representative of two independent experiments. **f**, ELISA of IL-1β from *Piezo1*$^{fl/fl}$ and *Piezo1*$^{\Delta LysM}$ BMDMs treated with CHP alone (NT), 10 ng ml^{-1} LPS with 5 h CHP followed by 1 h CHP, 5 h CHP followed by 1 h nigericin (10 μM) in CHP, or 10 ng ml^{-1} LPS for 5 h followed by 1 h nigericin (10 μM) with CHP. Data are presented as three biological replicates. Data in **c**, **d**, **f** are mean ± s.e.m.; significance is determined by unpaired two-tailed *t*-test (*$P < 0.05$, **$P < 0.01$, ***$P < 0.001$ and ****$P < 0.0001$).

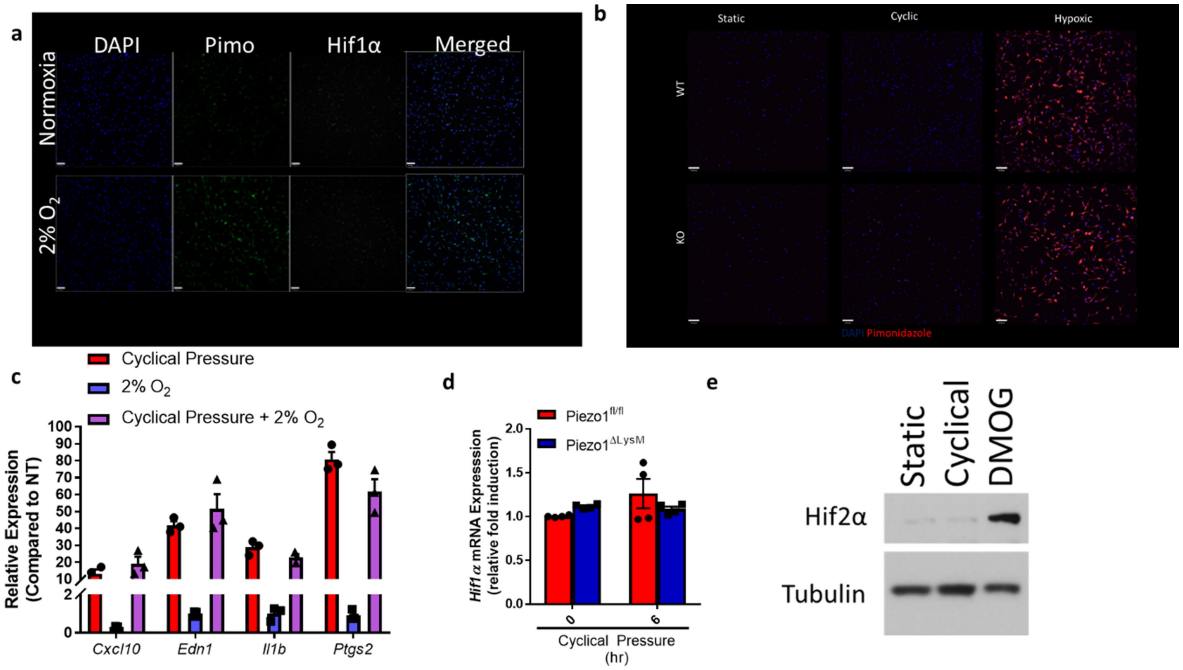

Extended Data Fig. 2 | HIF1α stabilization is independent of hypoxia during CHP stimulation. a, Representative confocal microscopy of BMDMs treated for 6 h in either normoxic conditions or in a hypoxic chamber (2% O_2). Cells were treated with pimonidazole (20 μM) for 1 h before completion of treatment. Upon completion, cells were fixed, permeabilized and stained with monoclonal antibody against pimonidazole. Data are representative of two independent experiments. **b**, Confocal microscopy of BMDMs treated for 6 h in either static, CHP or hypoxic chamber (0.5% O_2). Cells were treated with 20 μM pimonidazole 1 h before completion of treatment. Upon completion, cells were fixed, permeabilized and stained with monoclonal antibody against pimonidazole. Data are representative of two independent experiments. **c**, RT–qPCR analysis of BMDMs treated with cyclical hydrostatic pressure, 2% O_2 or cyclical hydrostatic pressure with 2% O_2 for 6 h. Data are presented as three biological replicates. **d**, RT–qPCR analysis of *Hif1a* in BMDMs following CHP. Data are presented as four biological replicates. Data are from two independent experiments. **e**, Representative immunoblot analysis of HIF2α and β-tubulin from BMDMs treated with static pressure, CHP or DMOG (200 μM) for 6 h. Data in **c**, **d** are mean ± s.e.m.; significance is determined by unpaired two-tailed *t*-test.

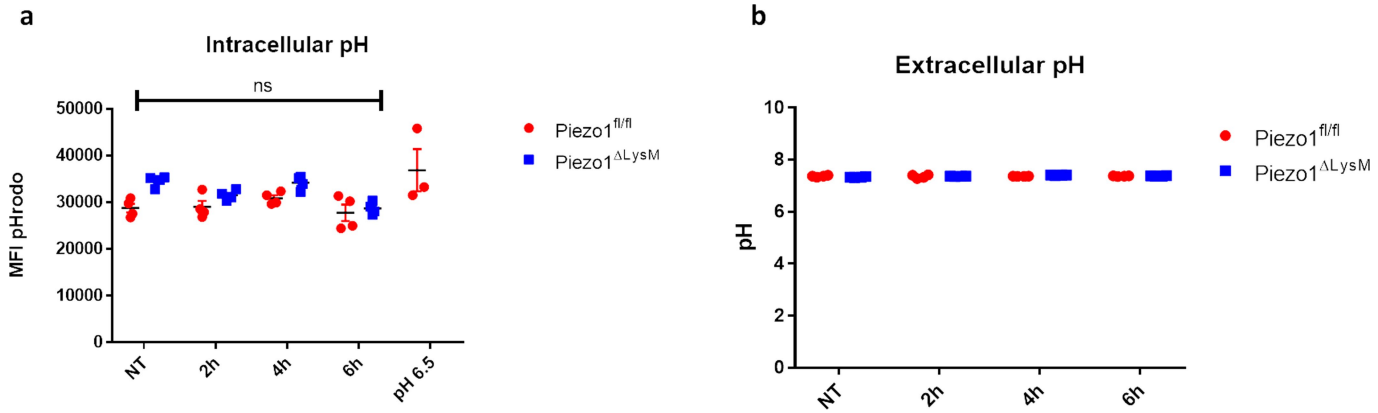

Extended Data Fig. 3 | Cyclical hydrostatic pressure-induced HIF1α protein is stabilized independent of acidity. a, Intracellular pH measurements using pHrodo intracellular pH indicator dye for final 30 min of treatment. *Piezo1*$^{fl/fl}$ ($n = 3$) and *Piezo1*$^{\Delta LysM}$ ($n = 3$) cells were treated with CHP for the indicated periods or with low-pH cell medium for 6 h. **b**, pH measurements of supernatant from *Piezo1*$^{fl/fl}$ ($n = 3$) and *Piezo1*$^{\Delta LysM}$ ($n = 3$) BMDM culture treated with CHP for the indicated periods. Data in **a**, **b**, are mean ± s.e.m.; significance is determined by unpaired two-tailed *t*-test.

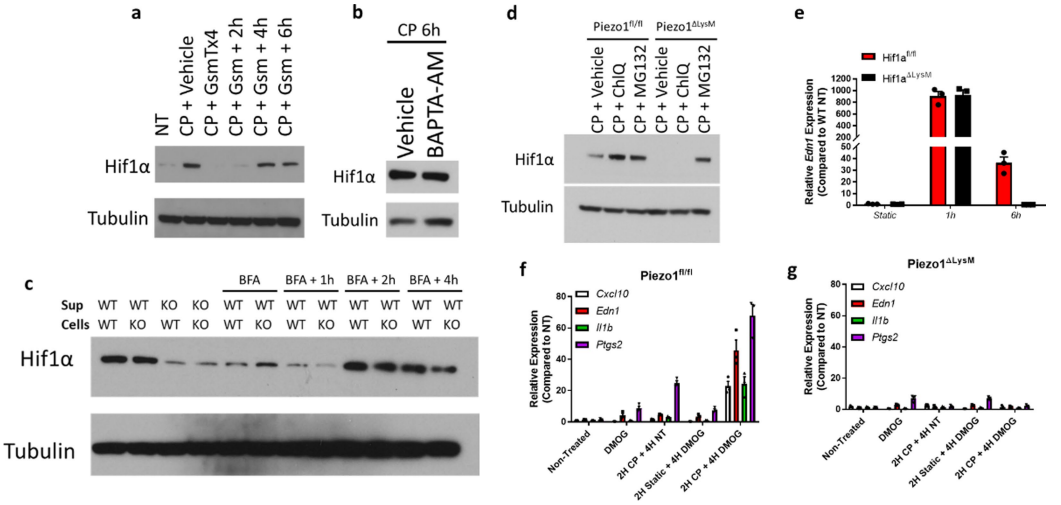

Extended Data Fig. 4 | Kinetics and sufficiency of cyclical hydrostatic pressure induced HIF1α stabilization and transcriptional response. **a**, Representative immunoblot analysis of HIF1α and β-tubulin from BMDMs in CHP with 5 μM GsMTx4 (Gsm) for 6 h, then washed three times in DMEM before further CHP stimulation. Data are representative of two independent experiments. **b**, Immunoblot analysis of HIF1α and β-tubulin from BMDMs in CHP for 6 h, pretreated with 10 μM BAPTA-AM for 30 min. Data are representative of two independent experiments. **c**, Immunoblot analysis of HIF1α and β-tubulin in BMDMs. *Piezo1*$^{fl/fl}$ (WT) or *Piezo1*$^{\Delta LysM}$ (KO) were cultured in CHP for 6 h along with 3 μg ml BFA. Cells were then washed with DMEM three times and further subjected to additional CHP stimulation. Supernatant (sup) was then clarified and transferred to WT or KO BMDMs cultured in static pressure for two additional hours. Data are representative of two independent experiments. **d**, Representative immunoblot analysis of HIF1α and β-tubulin from BMDMs treated with 100 μM chloroquine (ChlQ) or 50 μM MG132 for 6 h with CHP. Data are representative of two independent experiments. **e**, RT–qPCR analysis of *Edn1* from *Hif1a*$^{fl/fl}$ and *Piezo1*$^{\Delta LysM}$ BMDMs treated with CHP for 1 h or 6 h. Data are presented as three biological replicates. **f**, **g**, RT–qPCR analysis of *Piezo1*$^{fl/fl}$ (**f**) or *Piezo1*$^{\Delta LysM}$ (**g**) BMDMs cultured in 6 h of treatment 200 μM DMOG, 6 h of CHP, 2 h of CHP followed by 4 h of no treatment (NT), 2 h of static pressure followed by 4 h of 200 μM DMOG, or 2 h CHP followed by 4 h of 200 μM DMOG. Data are representative of three biological replicates. Data are mean ± s.e.m.

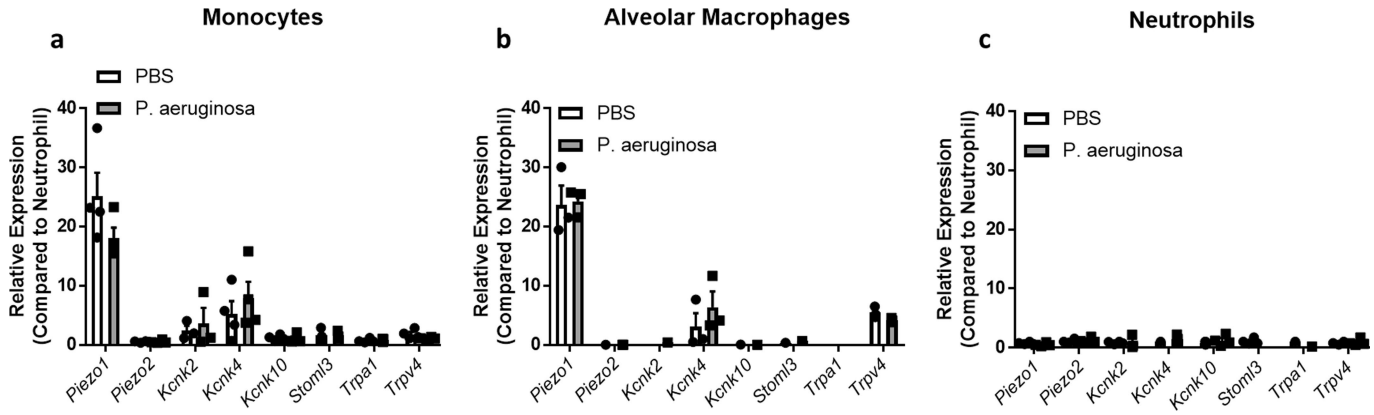

Extended Data Fig. 5 | Bacterial infection has no effect on MSIC expression. a–**c**, RT–qPCR analysis of known mammalian mechanosensory ion channels from monocytes (**a**), alveolar macrophages (**b**) or neutrophils (**c**) sorted from lungs of mice infected with *P. aeruginosa* or PBS for 6 h. Data are represented as fold increase over neutrophil expression for each gene. Data are representative of four biological replicates. Data are mean ± s.e.m.

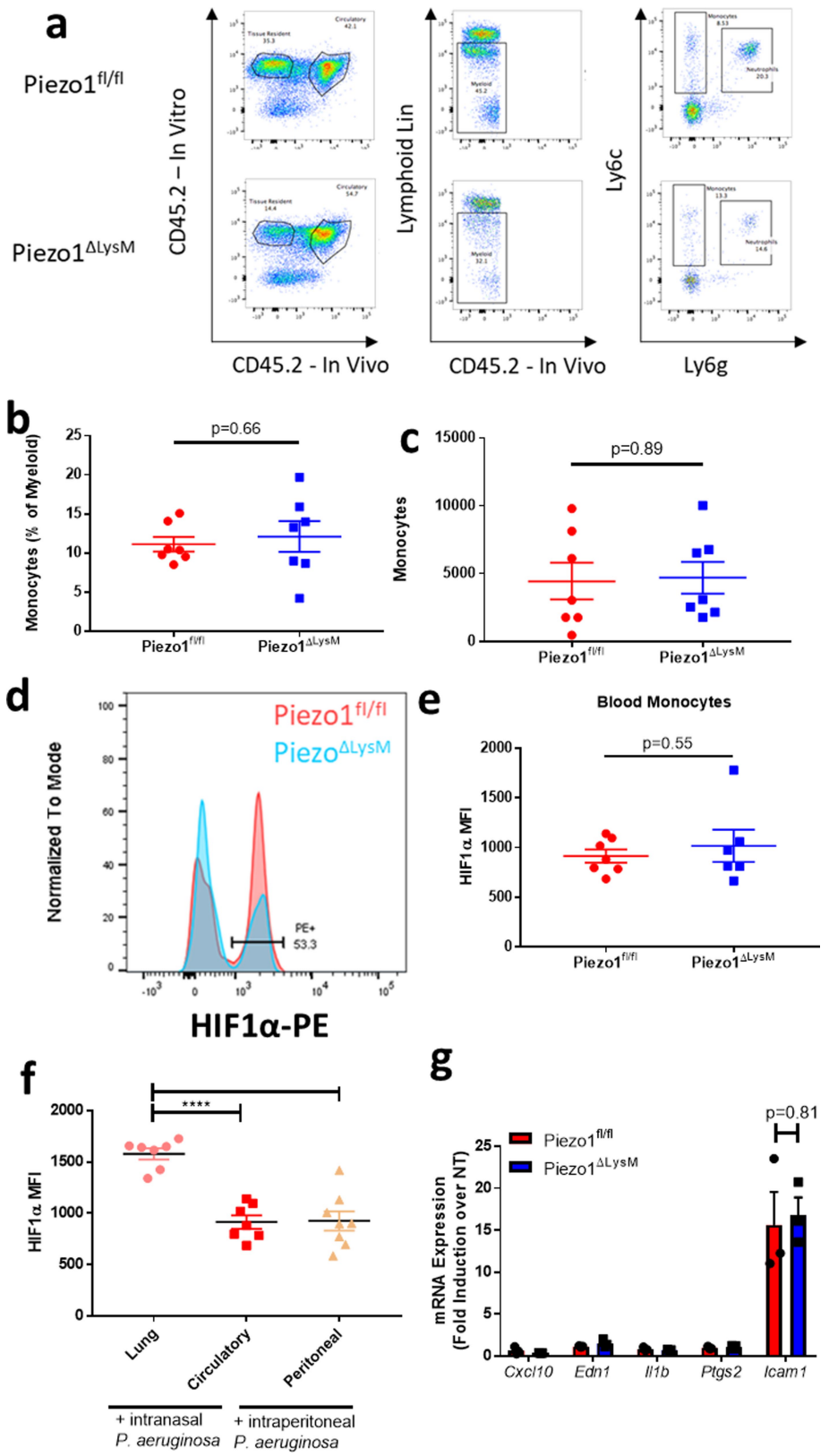

Extended Data Fig. 6 | See next page for caption.

Extended Data Fig. 6 | PIEZO1-dependent cyclical hydrostatic pressure stabilizes HIF1α in the lung. a, Representative flow cytometry of lungs from *Piezo1*$^{fl/fl}$ (top; $n = 9$) or *Piezo1*$^{\Delta LysM}$ (bottom; $n = 9$) mice infected intranasally with *P. aeruginosa* for 6 h. The lymphoid lineage is TCRβ$^+$NK1.1$^+$B220$^+$CD19$^+$CD90.2$^+$TCRγδ$^+$. Data are representative of two independent experiments. **b**, **c**, Infiltrating monocyte quantification in terms of percentage(**b**) and total numbers (**c**) following 6 h of intranasal *P. aeruginosa* infection of *Piezo1*$^{fl/fl}$ ($n = 7$) or *Piezo1*$^{\Delta LysM}$ ($n = 7$) mice. Data are representative of two independent experiments. **d**, Representative intracellular flow cytometry histograms of HIF1α from total lung interstitial monocytes of *Piezo1*$^{fl/fl}$ and *Piezo1*$^{\Delta LysM}$ mice infected intranasally with *P. aeruginosa* for 6 h. Data are from two independent experiments. **e**, MFI of HIF1α from in vivo-labelled CD45.2$^+$ circulatory monocytes from *Piezo1*$^{fl/fl}$ ($n = 7$) or *Piezo1*$^{\Delta LysM}$ ($n = 6$) mice infected with *P. aeruginosa* for 6 h. Data are from two independent experiments. **f**, MFI of HIF1α from tissue-infiltrated and circulatory monocytes from mice infected with *P aeruginosa* intranasally ($n = 7$) or intraperitoneally ($n = 8$) for 6 h. Data are from two independent experiments. **g**, RT–qPCR analysis from BMDMs treated with oscillatory shear stress for 6 h. Data are representative of three biological replicates. Data in **b**, **c**, **e**–**g** are mean ± s.e.m.; significance is determined by unpaired two-tailed *t*-test (****$P < 0.0001$).

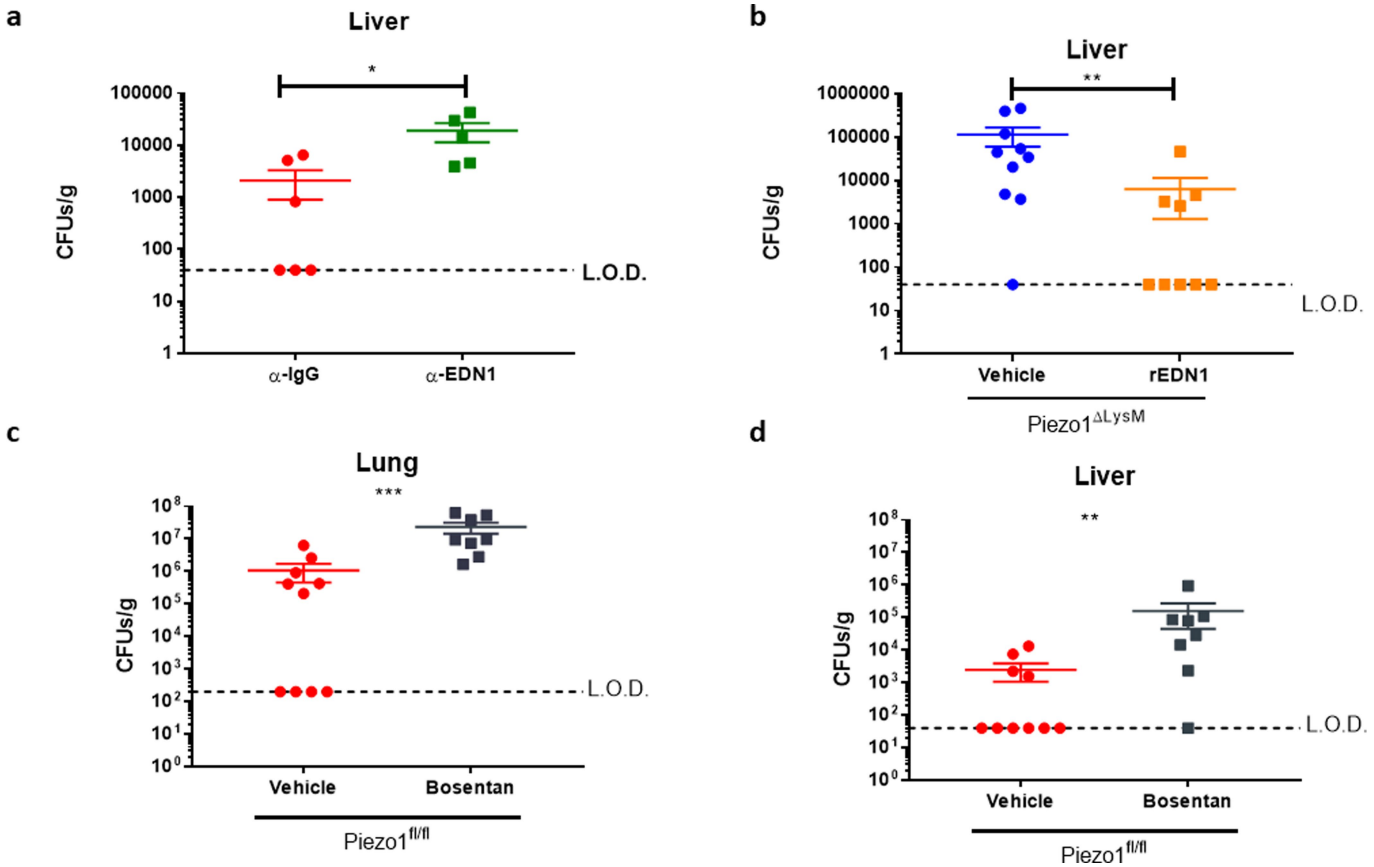

Extended Data Fig. 7 | EDN1 signalling confers protection to *P aeruginosa* infection. a, CFUs from liver of *Piezo1*$^{fl/fl}$ mice infected intranasally with *P. aeruginosa* for 24 h, pre-treated with 25 μg EDN1-blocking antibody ($n = 5$) or isotype control ($n = 6$) intranasally 6 h before infection. Data are from two independent experiments. **b**, CFUs from liver of *Piezo1*$^{\Delta LysM}$ mice infected intranasally with *P. aeruginosa* for 24 h treated with vehicle ($n = 10$) or 10 μg rEDN1 ($n = 9$) at the time of infection. Data are from two independent experiments. **c**, **d**, CFUs from lung(**c**) or liver(**d**) of *Piezo1*$^{fl/fl}$ mice infected intranasally with *P. aeruginosa* for 24 h, pre-treated with vehicle ($n = 10$) or 100 mg per kg (body weight) bosentan ($n = 8$) intraperitoneally 3 h before infection. Data are from two independent experiments. Data are mean ± s.e.m.; significance is determined by unpaired two-tailed Mann–Whitney *U*-test ($^*P < 0.05$,$^{**}P < 0.01$ and $^{***}P < 0.001$).

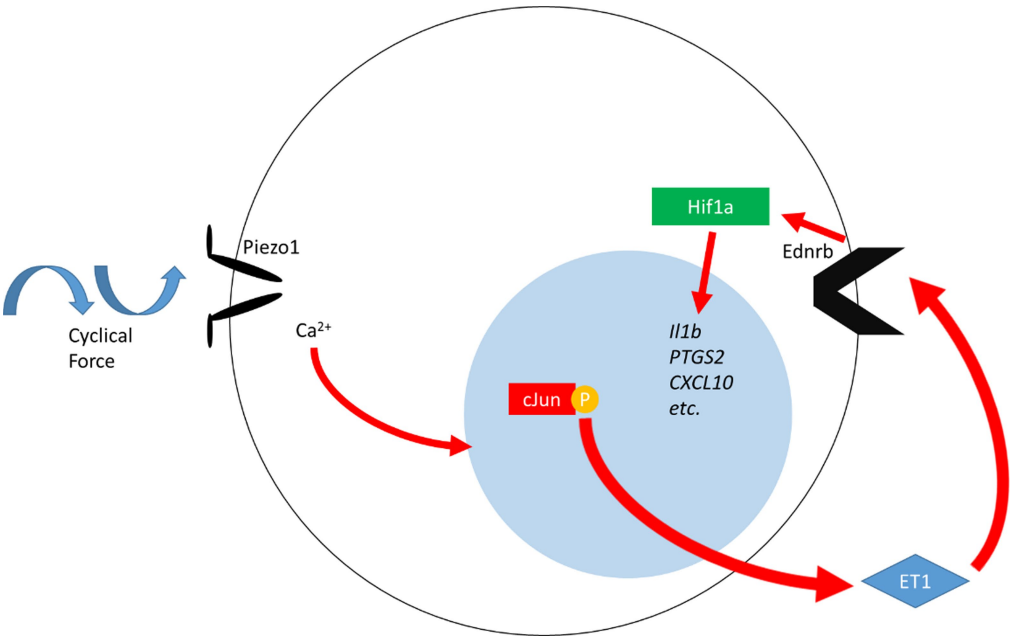

Extended Data Fig. 8 | PIEZO1 recognition of cyclical force drives a HIF1α proinflammatory program. Cyclical force signals via PIEZO1 in myeloid cells, resulting in Ca^{2+} influx and AP-1-induced EDN1 expression. Ednrb signalling then drives HIF1α stabilization and proinflammatory transcriptional upregulation.

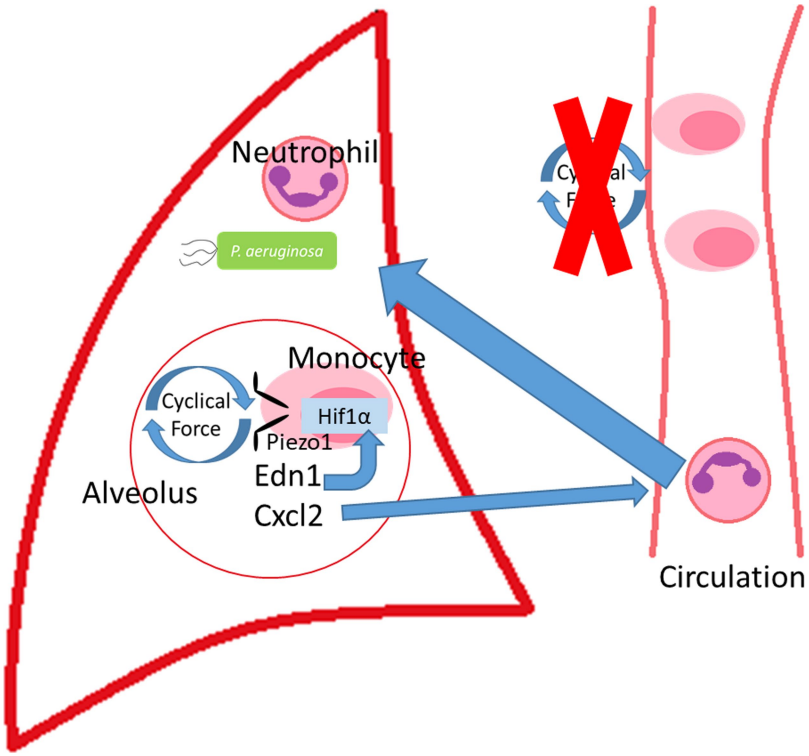

Extended Data Fig. 9 | Infiltrating monocytes recognize cyclical hydrostatic pressure in the lung via PIEZO1 to trigger neutrophil-mediated bacterial clearance. Recruited monocytes recognize cyclical force via PIEZO1 in the lung and secrete EDN1 to drive HIF1α stabilization and CXCL2 expression to induce neutrophilia and bacterial clearance.

nature research

Corresponding author(s): Angel G Solis, Ruaidhri P. Jackson, and Richard A. Flavell

Last updated by author(s): Jun 18, 2019

Reporting Summary

Nature Research wishes to improve the reproducibility of the work that we publish. This form provides structure for consistency and transparency in reporting. For further information on Nature Research policies, see Authors & Referees and the Editorial Policy Checklist.

Statistics

For all statistical analyses, confirm that the following items are present in the figure legend, table legend, main text, or Methods section.

n/a	Confirmed
☐	☒ The exact sample size (*n*) for each experimental group/condition, given as a discrete number and unit of measurement
☐	☒ A statement on whether measurements were taken from distinct samples or whether the same sample was measured repeatedly
☐	☒ The statistical test(s) used AND whether they are one- or two-sided *Only common tests should be described solely by name; describe more complex techniques in the Methods section.*
☐	☒ A description of all covariates tested
☐	☒ A description of any assumptions or corrections, such as tests of normality and adjustment for multiple comparisons
☐	☒ A full description of the statistical parameters including central tendency (e.g. means) or other basic estimates (e.g. regression coefficient) AND variation (e.g. standard deviation) or associated estimates of uncertainty (e.g. confidence intervals)
☐	☒ For null hypothesis testing, the test statistic (e.g. *F*, *t*, *r*) with confidence intervals, effect sizes, degrees of freedom and *P* value noted *Give P values as exact values whenever suitable.*
☒	☐ For Bayesian analysis, information on the choice of priors and Markov chain Monte Carlo settings
☒	☐ For hierarchical and complex designs, identification of the appropriate level for tests and full reporting of outcomes
☒	☐ Estimates of effect sizes (e.g. Cohen's *d*, Pearson's *r*), indicating how they were calculated

Our web collection on statistics for biologists contains articles on many of the points above.

Software and code

Policy information about availability of computer code

Data collection	qPCR data was collected using Bio-Rad CFX Manager v3.1. Flow cytometry data was collected using BD FacsDIVA v8.0.1.
Data analysis	Flow cytometry was analyzed using FlowJo v10. Confocal microscopy data was analyzed using Perkin Elmer Volocity (x64) v6.5. Figures were made using Graphpad Prism 7. Heatmap was made using Morpheus Open Software made available by the Broad Institute. RNA-sequencing analysis was conducted using R v. 3.5.0 using the CummeRbund package and CuffDiff2.

For manuscripts utilizing custom algorithms or software that are central to the research but not yet described in published literature, software must be made available to editors/reviewers. We strongly encourage code deposition in a community repository (e.g. GitHub). See the Nature Research guidelines for submitting code & software for further information.

Data

Policy information about availability of data

All manuscripts must include a data availability statement. This statement should provide the following information, where applicable:

- Accession codes, unique identifiers, or web links for publicly available datasets
- A list of figures that have associated raw data
- A description of any restrictions on data availability

RNA-sequencing data will be made available upon publication. Associated accession code is GSE133069

Field-specific reporting

Please select the one below that is the best fit for your research. If you are not sure, read the appropriate sections before making your selection.

☒ Life sciences ☐ Behavioural & social sciences ☐ Ecological, evolutionary & environmental sciences

For a reference copy of the document with all sections, see nature.com/documents/nr-reporting-summary-flat.pdf

Life sciences study design

All studies must disclose on these points even when the disclosure is negative.

Sample size	No sample-size calculations were performed. Sample sizes were determined by magnitude and consistency of measurable differences.
Data exclusions	No data was excluded.
Replication	All experiments were replicated to ensure data was reproducible.
Randomization	No formal randomization was done. Within experiments, mice were littermates, sex-matched, and age-matched.
Blinding	Investigators were blinded during counting of CFUs, but were not blinded during the processing of experimental samples.

Reporting for specific materials, systems and methods

We require information from authors about some types of materials, experimental systems and methods used in many studies. Here, indicate whether each material, system or method listed is relevant to your study. If you are not sure if a list item applies to your research, read the appropriate section before selecting a response.

Materials & experimental systems

n/a	Involved in the study
☐	☒ Antibodies
☐	☒ Eukaryotic cell lines
☒	☐ Palaeontology
☐	☒ Animals and other organisms
☒	☐ Human research participants
☒	☐ Clinical data

Methods

n/a	Involved in the study
☒	☐ ChIP-seq
☐	☒ Flow cytometry
☒	☐ MRI-based neuroimaging

Antibodies

Antibodies used	The following Biolegend antibodies were used: CD45.2 (clone 104, #109820, 109822, Lot B249623, B252126, 1:200), TCRβ (clone H97-597, #109212, Lot B211474, 1:1000), TCR γ/δ (clone GL3, #118116, B228498, 1:1000), NK1.1 (clone PK136, #108710, Lot B143114, 1:1000), B220 (clone RA3-6B2, #103212, 103206, 103224, 103208, Lot B242829, B230445, B246920, B136671, 1:200), CD19 (clone 6D5, #115512, Lot B248056, 1:1000), Ly6c (clone HK1.4, #128006, Lot B163395, 1:500), Ly6g (clone 1A8, #127614, 127624, Lot B156884, B264760, 1:200), CD169 (clone 3D6.112, #142407, Lot B210336, 1:150), Ter119 (clone Ly-76, #116212, Lot B213821, 1:1000), CD90.2 (clone 53-2.1, #553007, Lot 45519, 1:1000), CD11c (clone N418, #117308, 117318, Lot B234524, B251124, 1:150), and CD11b (clone M1/70, #101208, 101216, 101242, Lot B181098, B227804, B254686, 1:250), SiglecF (Clone E50-2440, #552126, Lot 7208832, 1:200). The following ThermoFisher antibodies were used: EDN1 (clone ENDO20-2101.70, #MA1-10818). The following Cell Signaling Technology antibodies were used: HIF1α (clone D2U3T, D1S7W, #14179S, 59370S, Lot 3, 1, 1:1000, 1:50), Hif2α (clone D9E3, #7096S, Lot 6, 1:1000), phospho-c-JUN (clones 54B3, D47G9, #2361S, 9164S, Lot 7, 5, 1:1000), phospho-JNK (clone 81E11, #4668S, Lot 14, 1:1000), total c-JUN (clone 60A8, #9165S, Lot 9, 1:1000) and total JNK (clone 9252, #9252S, Lot 8, 1:1000), Rabbit-HRT (#7074S, Lot 28, 1:2000). The following antibodies from Developmental Studies Hybridoma Bank were used: Beta Tubulin (clone E7, 1:3333). The following antibodies from GE Healthcare: Mouse-HRT (#GENA931, Lot 9761190, 1:2000)
Validation	For Biolegend antibodies CD45.2 (clone 104, #109820, 109822, Lot B249623, B252126, 1:200), TCRβ (clone H97-597, #109212, Lot B211474, 1:1000), TCR γ/δ (clone GL3, #118116, B228498, 1:1000), NK1.1 (clone PK136, #108710, Lot B143114, 1:1000), B220 (clone RA3-6B2, #103212, 103206, 103224, 103208, Lot B242829, B230445, B246920, B136671, 1:200), CD19 (clone 6D5, #115512, Lot B248056, 1:1000), Ly6c (clone HK1.4, #128006, Lot B163395, 1:500), Ly6g (clone 1A8, #127614, 127624, Lot B156884, B264760, 1:200), CD169 (clone 3D6.112, #142407, Lot B210336, 1:150), Ter119 (clone Ly-76, #116212, Lot B213821, 1:1000), CD90.2 (clone 53-2.1, #553007, Lot 45519, 1:1000), CD11c (clone N418, #117308, 117318, Lot B234524, B251124, 1:150), and CD11b (clone M1/70, #101208, 101216, 101242, Lot B181098, B227804, B254686, 1:250), SiglecF (Clone E50-2440, #552126, Lot 7208832, 1:200), manufacturer provided technical data sheets and validated antibodies for flow cytometry individually. For Cell Signaling Technology antibodies HIF1α (clone D2U3T, D1S7W, #14179S, 59370S, Lot 3, 1, 1:1000, 1:50), Hif2α (clone D9E3, #7096S, Lot 6, 1:1000), phospho-c-JUN (clones 54B3, D47G9, #2361S, 9164S, Lot 7, 5, 1:1000), phospho-JNK (clone 81E11, #4668S, Lot 14, 1:1000), total c-JUN (clone 60A8, #9165S, Lot 9, 1:1000) and total JNK (clone 9252, #9252S, Lot 8,

1:1000), Rabbit-HRP (#7074S, Lot 28, 1:2000), manufacturer provided certificate of analysis, and verified each antibody for western blot or flow cytometry individually. For ThermoFisher antibody EDN1 (clone ENDO20-2101.70, #MA1-10818), the manufacturer provided the certificate of analysis. For Developmental Studies Hybridoma Bank antibody Beta Tubulin (clone E7, 1:3333), manufacturer validated antibody for western blot use individually. For GE Healthcare antibody Mouse-HRP (#GENA931, Lot 9761190, 1:2000), manufacturer validated antibody for western blot use individually.

Eukaryotic cell lines

Policy information about cell lines

Cell line source(s)	293T (Susan Kaech, Salk Institute), Piezo1-floxed ES Cells (KOMP)
Authentication	293T cell lines were not authenticated. Genotype of Piezo1-floxed ES cells were authenticated via PCR.
Mycoplasma contamination	Cell lines were not tested for mycoplasma
Commonly misidentified lines (See ICLAC register)	N/A

Animals and other organisms

Policy information about studies involving animals; ARRIVE guidelines recommended for reporting animal research

Laboratory animals	Mice, strain C57Bl/6, males and females, 6-16 weeks of age.
Wild animals	None
Field-collected samples	None
Ethics oversight	All protocols in this manuscript have been approved by Yale IACUC

Note that full information on the approval of the study protocol must also be provided in the manuscript.

Flow Cytometry

Plots

Confirm that:

☒ The axis labels state the marker and fluorochrome used (e.g. CD4-FITC).

☒ The axis scales are clearly visible. Include numbers along axes only for bottom left plot of group (a 'group' is an analysis of identical markers).

☒ All plots are contour plots with outliers or pseudocolor plots.

☒ A numerical value for number of cells or percentage (with statistics) is provided.

Methodology

Sample preparation	Mice were sacrificed, and lungs were removed and placed in fresh media on ice. Cells were then finely chopped with clean dissection scissors, and digested with media containing collagenase D (Sigma) and DNase I (Sigma) for 30 minutes to an hour. Cells were then filtered through a 70um filter and pelleted. Epithelial cells were removed using an 80% to 40% Percoll (GE Healthcare) gradient spun at 600g for 20 minutes with slow acceleration and no brake. Cells between the gradient were removed and pelleted. Red blood cells were lysed using ACK Lysis Buffer. Cells were then stained for 30 minutes at 4°C.For intracellular staining, cells were fixed and permeablized using the Foxp3/Transcription Factor Staining Buffer Set (eBioscience™) exactly as described in the manufacturer's protocol. Cells were then filtered through a 40µM filter, and 20,000 counting beads were added. Samples were resuspended in PBS containing 2% FCS and 2mM EDTA and acquired with an LSRII cytometer (BD Bioscience).
Instrument	BD LSRII
Software	BD FacsDIVA and FlowJo.
Cell population abundance	Sample purity was verified as necessary
Gating strategy	Relevant gating strategy shown in figures.

☒ Tick this box to confirm that a figure exemplifying the gating strategy is provided in the Supplementary Information.